TECHNISCHE UNIVERSITÄT WIEN
Vienna University of Technology

Diplomarbeit

Studies of Adsorption on In_2O_3 (111) Surfaces

Ausgeführt am Institut für Angewandte Physik
der Technischen Universität Wien

unter der Anleitung von
Univ.Prof. Dipl.-Ing. Dr.techn. Ulrike Diebold
und Mag.rer.nat. Dr.rer.nat. Margareta Wagner

durch

Peter Lackner

Hede von Trappstraße 18 , 2100 Korneuburg

Abstract

This thesis describes scanning tunneling microscopy (STM) and photoelectron spectroscopy measurements of different adsorbates on the In_2O_3 (111) surface. STM measurements in ultra high vacuum show that water adsorbs at room temperature and forms features that are centered at specific sites in the unit cell. The saturation coverage observed in STM is one feature per unit cell. X-ray and ultraviolet photoelectron spectroscopy (XPS/UPS) results indicate OH-groups on the surface, albeit at higher coverages (two to six OH-groups per unit cell) than in STM. XPS results were also used to analyze the effects of increasing reduction of the In_2O_3 crystal. The evaporation of iron and nickel led to the formation of single adatoms. While the presence of iron on the surface could be confirmed through the use of Auger electron spectroscopy and low energy ion spectroscopy, it is unclear whether the adatoms are iron or indium atoms. At higher coverages disordered adatoms appeared, which could be ordered by annealing at 250 °C. Nickel evaporation led to disordered adatoms, which were surrounded by dark rings in STM images. This phenomenon can be explained by negatively charged adatoms. Preliminary investigations of organic molecules (6P and PTCDA) were also performed on the surface. At low coverages the molecules did not move during STM measurements. The evaporation of higher amounts of 6P led to a disordered overlayer.

Kurzfassung

Diese Diplomarbeit beschreibt Rastertunnelmikroskopie- (scanning tunneling microscopy, STM) und Photoelektronenspektroskopiemessungen verschiedener Adsorbate auf der In_2O_3 (111) Oberfläche. STM Messungen in Ultrahochvakuum zeigen, dass Wasser bei Raumtemperatur an der Oberfläche haftet. Die von Wasser erzeugten Objekte sitzen auf bestimmten Plätzen in der Einheitszelle. Die mit STM beobachtete maximale Bedeckung beträgt ein Objekt pro Einheitszelle. Messergebnisse von Röntgen- und Ultraviolettphotoelektronenspektroskopie (X-ray and ultraviolet photoelectron spectroscopy, XPS/UPS) zeigen, dass OH-Gruppen auf der Oberfläche gebildet werden. Allerdings beträgt die beobachtbare Bedeckung zwei bis sechs OH-Gruppen pro Einheitszelle, was nicht mit den STM-Ergebnissen übereinstimmt. Weiters wurden Teile der XPS Ergebnisse verwendet, um die Auswirkungen der Reduzierung des In_2O_3 Kristalls zu analysieren. Eisen wurde auf die Oberfläche gedampft, was zu geordneten Adatomen führte. Während durch Augerelektronenspektroskopiemessungen und niederenergetische Ionenstreuspektroskopiemessungen gezeigt werden konnte, dass sich Eisen an der Oberfläche befindet, ist weiterhin unklar ob die Adatome Eisen- oder Indiumatome sind. Bei höheren Bedeckungen bildeten sich ungeordnete Adatome, die durch das Erhitzen der Probe auf 250 °C geordnet werden konnten. Das Aufdampfen von Nickel führte zu ungeordneten Adatomen, welche von einem dunklen Ring umgeben waren. Dies konnte durch negativ geladene Adatome erklärt werden. Erste STM-Untersuchungen an organischen Molekülen (6P und PTCDA) zeigten, dass beide Molekülarten bei Raumtemperatur unbeweglich sind. Das Aufdampfen von größeren Mengen von 6P führte zu einer ungeordneten Molekülage.

Contents

Chapter 1

Introduction

Indium oxide (In_2O_3) features intriguing properties: It is transparent in the visual range of light as well as electrically conductive and therefore falls in the category of transparent conductive oxides (TCO). Moreover, its intrinsic conductivity can be enhanced by doping with tin, forming indium tin oxide (ITO). The level of doping is limited because it lowers the transparency of the material. The typical composition ratios In/Sn are between 95/5 and 90/10 wt%. Its transparency in the visual range lies between 80 and 95% [1]. Additionally, In_2O_3 features the possibility to be grown as a thin film on materials such as glass, mica or yttria-stabilized zirconia.

All these properties make indium oxide a perfect material for optoelectronic devices which require transparent substrates. Apart from applications such as gas sensors [2] it is therefore used in light emitting diodes (LEDs), thin film transistors [3], solar cells [4] as well as in coatings for smart windows [5]. As a result In_2O_3 has become more and more important in many fields. While both the demand for and the performance of devices using transparent oxides rise fast, basic interactions between the material and its adsorbates are not yet understood. An immense potential of rising efficiency awaits if the ongoing processes in such devices are better understood. Of particular importance are surface-adsorbate interactions, since they govern important properties such as the electron transfer efficiency.

Until recent years most research on ITO or pure In_2O_3 was done on thin films. While thin films are closer to the materials in the applications, measurements on single crystals benefit from defined morphology as well as enhanced regularity and stability. As our group has access to indium oxide single crystals these benefits can be used to approach this field of research from a new angle.

Three types of adsorbates are covered in this work, each of them with a different field of application: Water, organic molecules and metals. All three are useful for a better understanding of the indium

oxide surface itself. The interaction between water and the In_2O_3 surface is important for two reasons. On the one hand H_2O can be found in the residual gas of many ultra high vacuum chambers. Therefore it is essential to understand how these gas molecules change the surface. Otherwise all other results may be interpreted incorrectly. Water on the other hand will, as a part of the atmosphere, react with all indium oxide surfaces used in industry simply by handling them in an atmospheric or non-UHV environment. What is happening on an atomic scale is not yet understood.

The organic molecules used in this thesis, PTCDA and p-hexaphenyl, are typically used in OLED applications. Important properties can be investigated, e.g. the structure and adsorption site of the organic layer.

By depositing small amounts of metals on the In_2O_3 surface, phenomena such as the formation of clusters, agglomerations and single adatoms can be investigated. Single adatoms, similar to the indium adatoms on one of the surface terminations of In_2O_3 (111), could be used as model catalysts in the catalysis research [6, 7]. The metals used in this thesis, iron and nickel, are important catalysts in the industry. This research therefore features the possibility to understand catalytic processes better and increase the efficiency.

In addition to adsorption the effects of the reduction of In_2O_3 single crystals are studied. In_2O_3 as well as ITO thin films are often reduced. As a result they show an increase in oxygen vacancies. These vacancies influence the electronic states of neighboring atoms, which can be investigated using spectroscopic methods.

Chapter 2

Experimental Methods

2.1 Scanning Tunneling Microscopy (STM)

Scanning Tunneling Microscopy [8, 9] is making use of the quantum-mechanical tunneling effect. When two electrodes are in close proximity of each other, there is a certain probability that electrons can traverse from one electrode to the other. If a voltage U_{B} is applied between the two materials, electrons of the cathode tunnel into the anode. As a result a tunneling current can be measured which is dependent on the distance z and the local density of states (DoS).

In the experiment a sharp tip is moved close enough to the surface so that electrons can tunnel from the surface to the tip, or vice versa, depending on the voltage. If for example a positive voltage is applied, electrons tunnel from the conduction band of the tip into filled states of the sample.

There are two modes of measurement. In the constant height mode the height z of the tip is held at a reference level and the current is recorded. In the constant current mode, which is used in this thesis, the current is kept constant via a feedback loop. The displacement of the tip is constantly adapted and recorded. On a flat surface, the tip moves closer when the local DoS decreases, since the tunneling current decreases. When the local DoS increases, the tip moves further away. On a rough surface, the tip additionally follows the height of the surface. This movement is recorded while the tip is moving across the surface in x and y direction. Tip movements are realized by piezo elements, in combination with a feedback loop.

The resulting array of data can be used to create images of the surface which ideally provide atomic resolution. This image is a superposition of the real space height and the electron DoS. A bright spot for example could be an atom sticking out of the surface, but also an area with a higher DoS.

An ideal STM tip would be so sharp that there is a single atom at the very end. Many typical

problems of this method arise because of imperfect tip conditions:

- Blunt tip: Features such as single atoms or step edges are blurred. In some cases they are not discernible at all.

- Double or multiple tip: Images show overlapping or double features, since the image is a convolution of the tip's shape and the surface. This can lead to strongly delusive images.

- Changing tip conditions: The tip needs to be stable to get reliable data, which is not always easily achieved.

- The unknown tip apex makes the interpretation difficult. Usually neither its shape nor its consistency is known for certain.

- Further interpretation problems can occur since the electron density and height of the surface are measured at the same time and can not easily be distinguished, as mentioned above.

In our setup we use two different STMs, see chapter 2.3, and electro-chemically etched tungsten tips. The bias voltage is applied to the sample. The sample bias and current levels used for a specific image in this work are given in the respective figure caption. Typical values for tunneling currents lie between 0.1 and 0.3 nA, for voltages between ± 0.5 and ± 2.5 V. Electrons tunnel into empty states of the sample at positive biases.

The STM raw data can be found using the file names given in the figure captions. The file structure is divided into Omega and RT measurements, and further divided into folders for every crystal. Measurements on crystal number 2 have file numbers between 0200 and 3000, measurements on crystal 1 in RT have file numbers above 10000. Other file numbers are given to measurements in Omega on crystal 1 and 4.

2.2 Spectroscopic Methods

The chemical composition of the surface was investigated using different complementary spectroscopic methods. These methods vary in surface sensitivity, measured surface area and damage done to the sample.

2.2.1 X-Ray Photoelectron Spectroscopy (XPS)

The aim of an XPS [10, 11, 12] measurement is to get information about the binding energies of core electrons, which are unique for each element. To extract the electrons, photons with an energy of hν greater than the binding energy are irradiated at a sample. The photons penetrate several µm deep into the material and ionize atoms. The excited electrons with an energy higher than the work function of the material, $h\nu > E_B + \Phi_S$, can leave the sample. They are measured using an electron detector. Since the photon energy is known and the kinetic energy of the electron is measured, the binding energy can be calculated using

$$E_B = h\nu - E_{kin} - \Phi_A,$$

where Φ_A is the work function of the analyzer. For a more detailed description of the energy levels involved in XPS measurements, see [11].

The photoelectrons can travel a certain average distance in the material before being inelastically scattered - the so-called inelastic mean free path or IMFP. If an electron is scattered elastically, the energy stays constant and the electron still contributes to the correct binding energy peak. If, on the other hand, an electron gets scattered inelastically it only raises the background. For this reason the IMFP is a realistic measure for the surface sensitivity of this method. It is energy dependent, see figure 2.1, and ranges from 5 to 15 Å for energies between 60 and 1250 eV, which is the energy range used in the measurements in this thesis. This makes XPS a surface sensitive method. The surface sensitivity can be increased further by measuring in grazing emission.

The measured spectrum shows the characteristic peaks of all elements present on the surface combined. Auger peaks (see Auger electron spectroscopy, section 2.2.2) are also measured. In addition to the identification of the elemental composition of the surface, the spectrum allows the quantification of the concentration of different elements by comparing the peak area. Since different elements have a different sensitivity to ionizing radiation, this has to be taken into account by using so-called atomic sensitivity factors. Furthermore the position of peaks can be used to gain information regarding the chemical environment of the measured atoms. For example the binding energy of the electrons of a metal typically increases with its oxidation state. This is called chemical shift.

The typical photon source in a laboratory is a non monochromatic X-ray tube with aluminium or magnesium targets. Instead of an X-ray tube, different photon sources can be used. Most measurements in this thesis were done at the MAXII storage ring in Lund, beam line I311 [13], where synchrotron radiation was available. This kind of radiation is created in particle (usually electron)

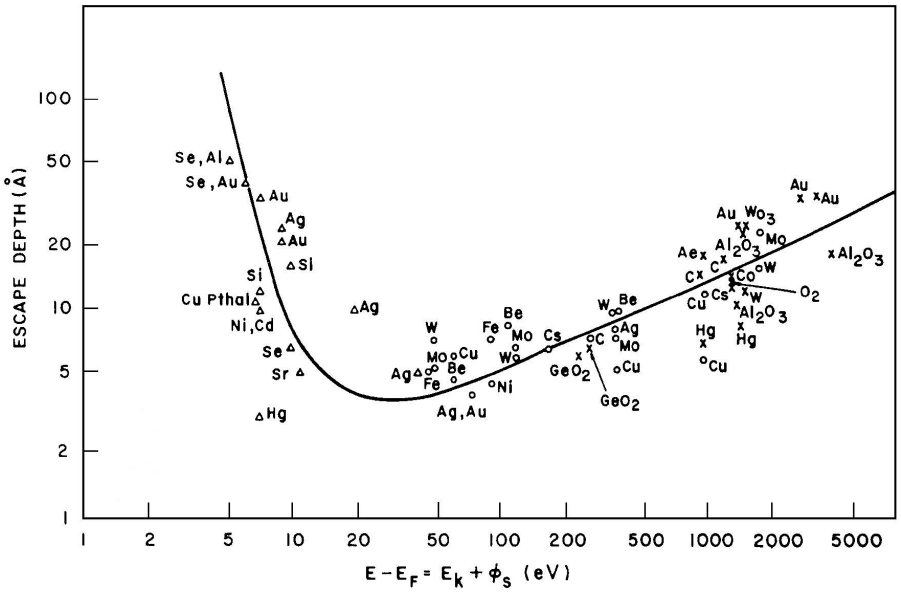

Figure 2.1: Diagram showing the electron escape depth as a function of the electron energy. Taken from [11].

storage rings when the particles are diverted in the magnetic field of a bending magnet, undulator or wiggler. This type of radiation source has many advantages:

- The intensity is much higher compared to an X-ray tube. As a result measurements take less time and have a better signal to noise ratio.

- Variable photon energy. When using an undulator (as we did), the gap between the magnets can be changed to adjust the photon frequency. It can therefore be set to be near the energy range that is interesting for the present measurement. Typically the energy is set to $E_B + 200\,eV$ to be as surface sensitive as possible while still avoiding the higher background from secondary electrons. This arises when measuring binding energies near the photon energy. The used photon energy is always mentioned in the respective figures or figure captions.

- The photon energy can be changed to very low values, 42.5 eV minimum in the case of beamline I311, allowing measurements of the valence band similar to ultraviolet photoelectron spectroscopy (UPS).

- The photons have a very narrow energy distribution because they pass a monochromator before hitting the sample.

- The beam can be focussed on a very small area. This is important when trying to measure the sample without any influence from the sample plate and holders. At beamline I311 at Max-Lab the area was 0.5 (horizontal) x 0.2 (vertically) mm^2 at normal incidence.

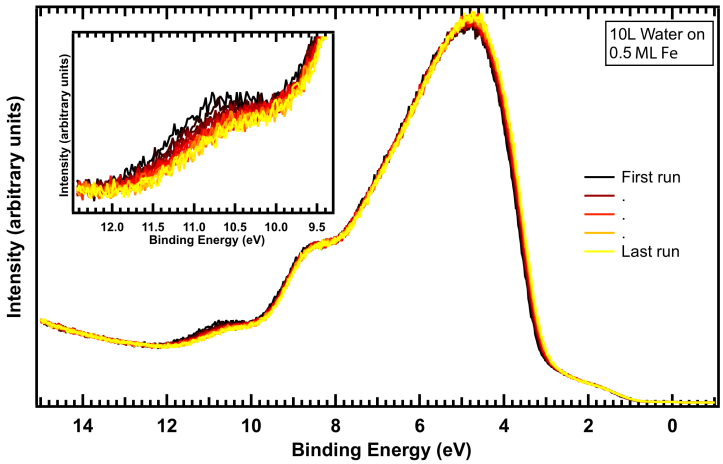

Figure 2.2: Valence band measurement of the oxidized surface of In_2O_3 after evaporation of 0.5 ML of iron followed by 10 L of water. The peak at 10.7 eV that is created by water interacting with the surface is gradually weakening. After 14 sweeps a significant decrease is visible. The measurement was made at a photon energy of 60 eV.

- Extremely high brilliance, i.e. a high number of photons per second as well as small collimation, source area and spectral distribution [14].

The raised intensity also raises the destructiveness of the method. An example is shown in figure 2.2, where water was dosed on an iron covered oxidized surface of indium oxide. The valence band measurement shows that the water signal is decreasing over time. This effect is normally eased by exposing the sample only for the minimal time or by focussing the beam at a different position after every measurement.

Our setup in the lab included an X-ray gun using Mg Kα radiation at 1254 eV, the radiated sample and a hemispherical analyzer. At the synchrotron facility synchrotron radiation was used. The photon energy was varied and is given in the figures.

2.2.2 Auger Electron Spectroscopy (AES)

The Auger effect, on which AES [15] relies, can be described as follows: If a core electron is excited, an electron from an upper shell can fill the newly created hole. The excessive energy is transferred via a radiation-free process to a third electron which is also excited. The Auger process is therefore a three-electron process. In the end, two electrons have been freed: The initial core electron and the so called Auger electron. The Auger electrons have distinct energies, which only depend on the shells in which the contributing electrons were, but not on the energy of the incident particle which exited the first electron.

Example: A K-electron is ionized and an L_I-electron fills the hole. Through the Auger effect an

L_{II}-electron is freed. The kinetic energy of this electron is, to first approximation,

$$E_{kin} = E_K - (E_{L_I} + E_{L_{II}}) - \Phi,$$

where Φ is the work function of the sample.

In the case of Auger electron spectroscopy the excitation of the core electron is induced by high energy electrons (typically 2 to 10 keV, in our case 3 keV) shot at the sample. Similar to XPS the escaping electrons are measured, but in this case the kinetic energy must only be corrected by the work function since the kinetic energy is not influenced by the energy of the incoming electron.

The result is a spectrum of intensity versus kinetic energy. It is normally differentiated to pronounce small peaks and suppress the background. The background is very high due to inelastically scattered primary, secondary and Auger electrons. The Auger peaks are again typical for every element.

Analogous to X-ray photoelectron spectroscopy, AES is surface sensitive because of the inelastic mean free path of the excited electrons, see section 2.2.1. In the case if AES also the incoming particles are electrons, which raises the surface sensitivity further. Since the Auger effect is a three-electron effect hydrogen and helium can not be detected.

Our setup consisted of an electron gun (emission current of 1 mA), the sample and a cylindrical mirror analyzer. All AES measurements in this work were done under an angle of approximately 30° to the surface normal.

2.2.3 Low Energy Ion Scattering (LEIS)

LEIS [16], also called Ion Scattering Spectroscopy (ISS), is a method for determining the masses of atoms present on the sample surface. The method relies on inelastic collisions between atoms. Ions, typically He^+, are propelled at the surface and collide with the topmost atoms. The energies after the collision depend on the masses of the collision partners. The higher the mass difference between atom and ion, the higher the energy of the ion after the collision. The difference in energy gets smaller with higher masses, therefore it is harder to distinguish heavy surface atoms when their masses are similar. The energy of the reflected ions is measured and a spectrum of intensity over kinetic energy is created.

The big advantage of this method is its extreme surface sensitivity. Since only electrically charged ions are measured in the analyzer, collisions that result in the neutralization of the ion are not counted. The neutralization probability in a collision is higher than 99% [11], so the probability to measure an ion falls sharply with the number of collisions, and therefore with the depth. Because of this it can be assumed that only the top layer is being measured.

The main disadvantage comes with the principle of ion bombardment. Although light helium ions are usually used in LEIS, the bombardment damages the topmost layer. This leads to the problem that elements present only in the topmost layer can only be measured in the first seconds of the measurement, as they are sputtered away or pushed deeper into the material. However a quickly vanishing signal can always be attributed to an element only present on the surface.

The experimental setup included an ion gun that propelled He^+ ions with an energy of 1025 eV, the sample and a hemispherical analyzer. The scattering angle was 90°. The beam was as focussed as possible (setting: 0x0 mm^2). The typical He pressure used was $4.2 \cdot 10^{-7}$ mbar. Using this settings the target current is typically around 1 µA.

2.3 Ultra High Vacuum Systems

Measurements were taken in two ultra high vacuum (UHV) systems. The main system ("Omega") was not equipped with a separated preparation chamber, which led to a base pressure of below $3 \cdot 10^{-10}$ mbar. The chamber was equipped with an STM (Omicron STM-1) and could be used for XPS measurements. An hemispherical analyzer SPECS PHOIBOS 100 was used in combination with a non monochromatic Mg Kα X-ray gun emitting photons at an energy of 1254 eV. The chamber could be equipped with an Omicron Focus EFM3 single evaporator [17] for iron deposition or an OmniVac 4-pocket molecule evaporator [18], whichever was needed.

The second system ("room temperature" or "RT") had two separate chambers, one for preparation and a main chamber for measurements. The base pressure in the preparation chamber was below $1 \cdot 10^{-10}$ mbar. The base pressure in the main chamber was below $7 \cdot 10^{-11}$ mbar. It was equipped with:

- AES, using a Perkin-Elmer electron gun (model 11-010) and Perkin-Elmer cylindrical mirror analyzer (Model 10-155)
- LEIS, using a SPECS IQE 12/38 ion gun and a SPECS Hemispherical Analyser EA10 Plus
- STM, using an Omicron µSTM

Iron and nickel could be deposited using a LN_2-cooled Omicron Focus triple evaporator in the preparation chamber.

The only measurements taken in a different system were the spectroscopic measurements done at the synchrotron facility Max-Lab in Lund. The base pressure in the preparation chamber was

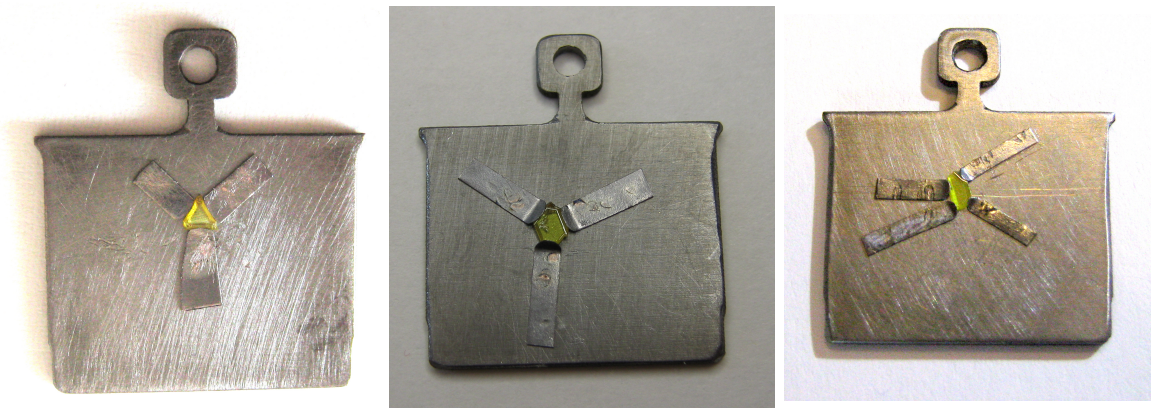

Figure 2.3: Crystals on SPECS tantalum sample plates held by tantalum clips. From left to right: Crystal number 1, 2 and 4

between the mid or high 10^{-10} mbar range. The background pressure in the analysis chamber was below $1 \cdot 10^{-9}$ mbar.

2.4 Sample Preparation

2.4.1 Crystals

The experiments described in this work were conducted on three In_2O_3 single crystals. They were grown in the lab of Dr. Lynn A. Boatner, Oak Ridge National Laboratory, and were cut and polished in (111) direction by the company SurfaceNet GmbH. The surface area and shape varied between the crystals:

- Crystal number 1 was a triangle with a side length of 1 mm.
- Crystal number 2 was a hexagon with a diameter of 2 mm.
- Crystal number 4 was a rectangle with side lengths of 2 x 1 mm and a broken edge.

The height of all crystals was around 0.5 mm. Tantalum clips were used to secure the specimen on SPECS tantalum sample holders. See figure 2.3 for pictures of the mounted crystals.

2.4.2 Cleaning the Sample

The daily cleaning procedure of the In_2O_3 (111) surface typically started with 10 minutes of sputtering (10^{-6} mbar Ar^+, 1 keV, 1.5 µA) followed by 10 minutes of annealing at 425°C and another 10 minutes of sputtering. The second annealing cycle was varied for different surface preparations:

- For the bulk terminated (so-called oxidized) surface the sample was annealed in an O_2 pressure of $1 \cdot 10^{-7}$ mbar at 425°C for 10 minutes and cooled down in oxygen to 150°C .

- For the surface covered with a full monolayer of indium adatoms ("reduced surface") the sample was annealed for 10 minutes in UHV.

- For a surface partially covered with indium adatoms the sample was annealed as for the bulk terminated surface, but in a different oxygen pressure. $1.5 \cdot 10^{-8}$ mbar for example led to a coverage of approximately 20%, i.e. one indium atom every five unit cells.

The preparation procedures are based on prior work in the group, see chapter 3.2 and [19].

In case of large amounts of deposited material on the surface from previous preparations, the first sputtering cycle was extended to 20 minutes. When the sample was exposed to air it was cleaned with approximately eight cycles after inserting it into the UHV chamber.

After the last annealing cycle the sample was left in the manipulator to cool down to below 55°C to avoid temperature induced drift in STM measurements. The cleanliness of the sample was checked with STM.

2.4.3 Water Dosing

Water vapor was dosed into the vacuum chamber. This had the advantage that the sample could stay in the STM while dosing. This allowed us to check the condition of the surface during or right after the interaction. Typically pressures between $1 \cdot 10^{-9}$ and $1 \cdot 10^{-8}$ mbar were used. The water source was distilled water which was cleaned by several cycles of freeze pumping.

The water dosage is given in Langmuir (L), and is equivalent to a pressure of $1 \cdot 10^{-6}$ torr for one second. Assuming a sticking coefficient of 1, 1 L leads to a coverage of a full layer.

The dosage values given in this thesis include the rise and fall time during dosing. The main source of error are pressure instabilities during dosing. This error can be pessimistically estimated as 5% of the mean dosage value. Furthermore the water was pumped out of the chamber very slowly, thus a background pressure in the 10^{-10} mbar range stayed for longer than an hour. This however did not influence our dosage, as no reactions were observed in the measured area below the STM tip. Outside this area the coverage continued to rise.

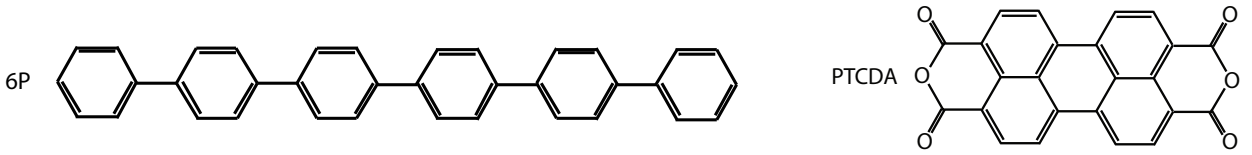

Figure 2.4: Conjugated organic molecules used in this work. P-hexaphenyl (left) has a sublimation temperature of 260°C, PTCDA (right) sublimates at 435°C.

2.4.4 Iron Evaporation

For evaporating iron we used an Omicron Focus EFM3 single evaporator [17]. The operation mode is based on a filament which is heated by a current of approximately 2 A. The iron rod inside the evaporator was set to a high potential of typically +800 V. The high electric field between filament and iron rod propelled electrons towards the iron rod, which was heated by the impacts. Iron atoms evaporated from the rod, through the orifice and into the chamber. The emission current was measured to monitor the heating power. During evaporation the flux (the amount of ionized particles, which is proportional to the total amount of evaporated particles) was held constant.

The deposition rate was measured with a quartz crystal microbalance (QCM) with standard settings (Z-factor 1, density 1, tooling 100). It was heated to 87 °C for stability against temperature variations. The coverage was calibrated with the STM by counting the deposited atoms. In this thesis the coverage is given in monolayers, which in this context means one adatom per unit cell. One monolayer corresponds to a coverage of $5.88 \cdot 10^{13}$ atoms/cm^2.

2.4.5 Molecule Evaporation

The evaporation of different organic molecules was done using an OmniVac 4-pocket evaporator [18]. It provided four crucibles which could be heated separately. They were filled with molecule powder and heated to the sublimation temperature or just below to start evaporation. The deposited amount was measured with a QCM.

The molecules we used were PTCDA and p-hexaphenyl, see figure 2.4. The evaporation temperatures were 435°C and 260°C, respectively. The van der Waals size of 6P is 6.7 Å · 27.2 Å [20]. The size of PTCDA is 14.2 Å · 9.2 Å [21].

Chapter 3

Previous Results

3.1 The In_2O_3 Crystals

In_2O_3 forms yellow, transparent crystals. It crystallizes in the bixbyite structure [22]. The unit cell contains 32 indium and 48 oxygen atoms and has a lattice constant of 1.01150(5) nm [23].

The high-purity crystals used in this work were characterized by Hagleitner *et al.* [23]. Impurities that were found were Pb (4307 ± 74 ppm), Mg (1388 ± 42 ppm) and Pt (155 ± 28 ppm). Depth profiles approximately 2000 nm deep showed that the impurity distribution was uniform.

The band gap was investigated by King *et al.* [24]. They derived a value for the fundamental band gap from the measured optical absorption coefficient as 2.93 ± 0.15 eV. It is typically assumed that In_2O_3 is n-doped due to oxygen vacancies [25]. In our case the influence of impurities can also not be excluded as a reason.

3.2 The Two Terminations of the In_2O_3 (111) Surface

Wagner *et al.* [19] reported on two different surface terminations of the In_2O_3 (111) surface, see figure 3.1 (a1) and (a2). The first termination resulted from annealing in $1 \cdot 10^{-7}$ mbar of oxygen at 500° C and was thus called "oxidized surface termination". It exhibits dark, triangle-shaped features in STM. The second termination, resulting from annealing in UHV at 500° C, shows a (1x1) overlayer of bright protrusions, which were identified as indium adatoms. These adatoms sit in the middle of the dark triangle features, which appear on the oxidized termination. Due to the reducing conditions during the preparation this termination was named "reduced surface termination". Intermediate terminations with a partial indium adatom coverage were also prepared and shown. They are called "partially

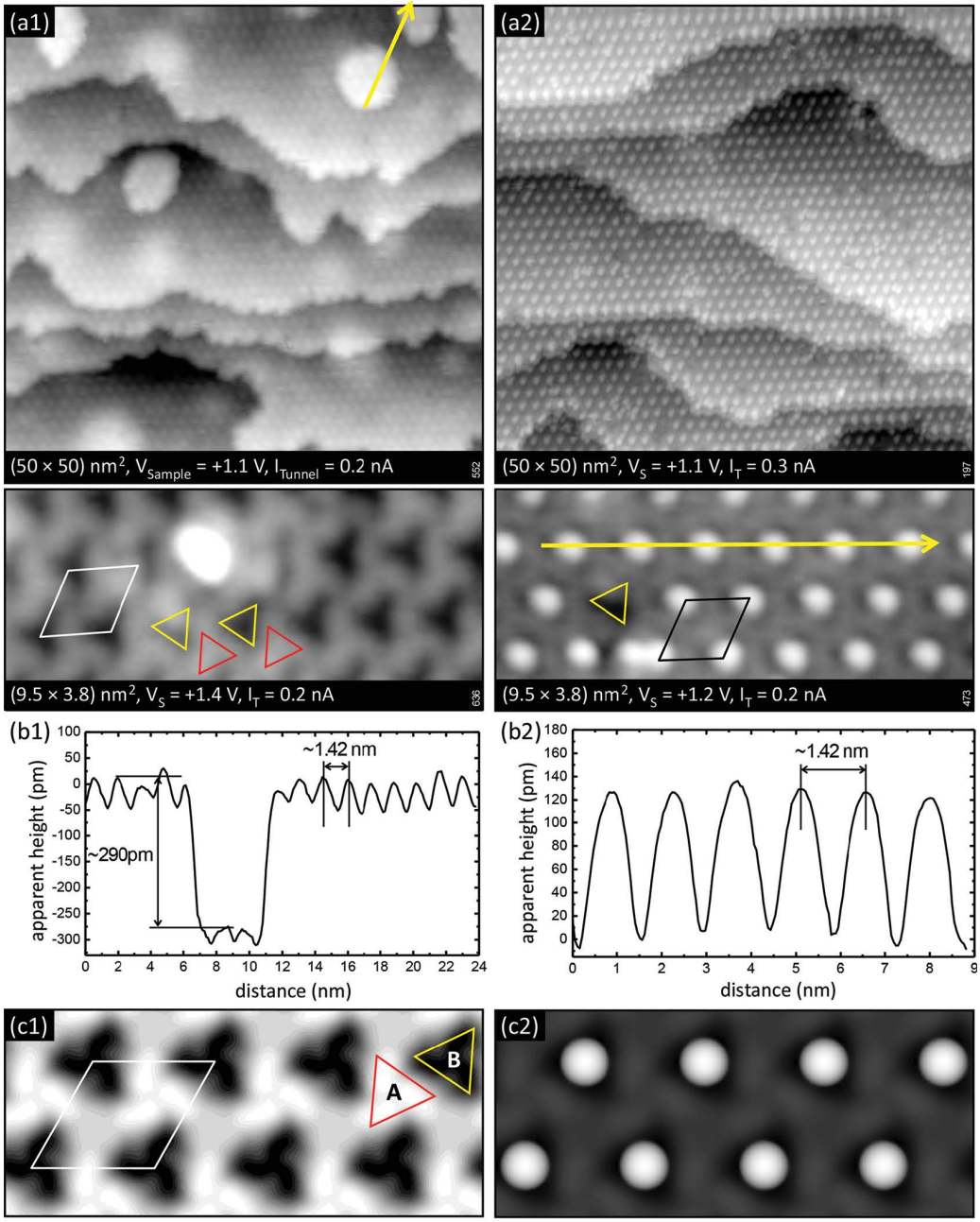

Figure 3.1: STM images of the two surface terminations of In_2O_3 (111) from [19]. The oxidized termination (left) and the reduced termination (right) are presented with measurements (two top rows), line profiles (middle) and calculated STM images (bottom). Both surfaces show the same periodicity. They differ only by the indium adatoms on top of the dark triangles. The step height is approximately 290 pm in both cases. The corrugation is 60 pm for the oxidized and 120 pm for the reduced surface. The STM measurements are in good agreement with DFT calculations.

reduced surfaces" in this work. STM images calculated using DFT agree with the measurements, as can be seen in figure 3.1 (c1) and (c2).

Figure 3.1 (b1) and (b2) show line profiles of the two terminations. The step height was circa 290 nm. The corrugation of the oxidized surface was 60 pm. Indium adatoms had an apparent height of 120 pm.

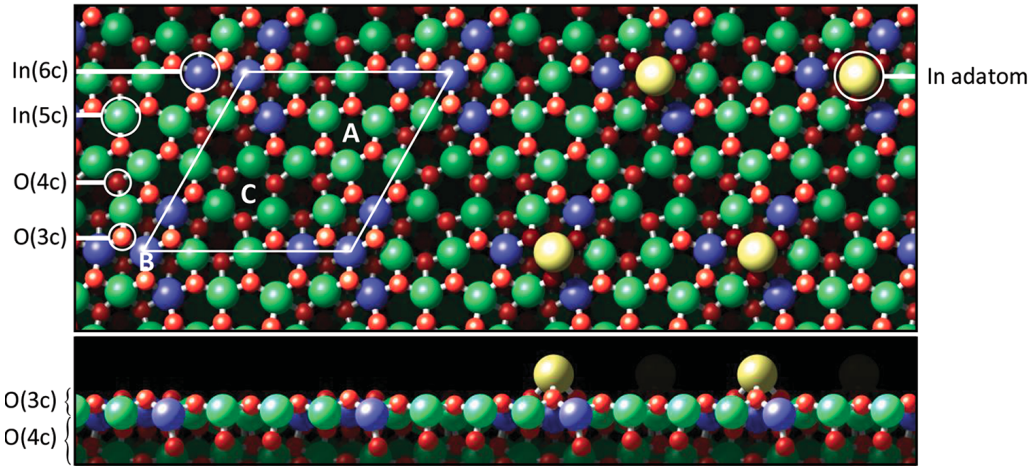

Figure 3.2: Model of the two surface terminations of In_2O_3 (111) by [19]. On the left side the oxidized termination is shown, on the right side the reduced termination is shown. The unit cell is marked in white. The oxygen atoms are colored red, where bright red means threefold coordination and dark red means fourfold. Fivefold-coordinated indium atoms are colored green, sixfold-coordinated blue and adatoms yellow. The brightness of the green adatoms depicts at which height they are located, the brighter the higher.
High symmetry positions are pointed out. A and C are rings of indium and oxygen atoms. B is the center of the dark triangle feature measured in STM.

Using DFT calculations and the above mentioned STM images, Wagner *et al.* derived models of both surface terminations, see figure 3.2. Both feature a rhombical unit cell with a side length of 1.43 nm and a hexagonal symmetry. When calculating theoretical STM images, the authors found that the dark triangles were located at the sixfold-coordinated indium atoms, which are colored in blue in the model. The indium adatoms sat on top of the middle atom or in one of the three oxygen bridge sites nearby.

Morales *et al.* [26] measured fully oxidized Sn-doped In_2O_3 films. Their films were grown in an oxygen plasma background and were doped with 2.4, 4.1 and 6.2 atomic percent of Sn. The resulting STM images, see figure 3.3, feature the oxidized surface termination reported by Wagner *et al.* with the same corrugation and periodicity. Due to the film growth domain boundaries are formed.

Zhang *et al.* [27] annealed In_2O_3 thin films in UHV at 600 °C. They reported STM images featuring protrusions similar to the reduced surface, see figure 3.4. The images are in good agreement to the findings of Wagner *et al.*

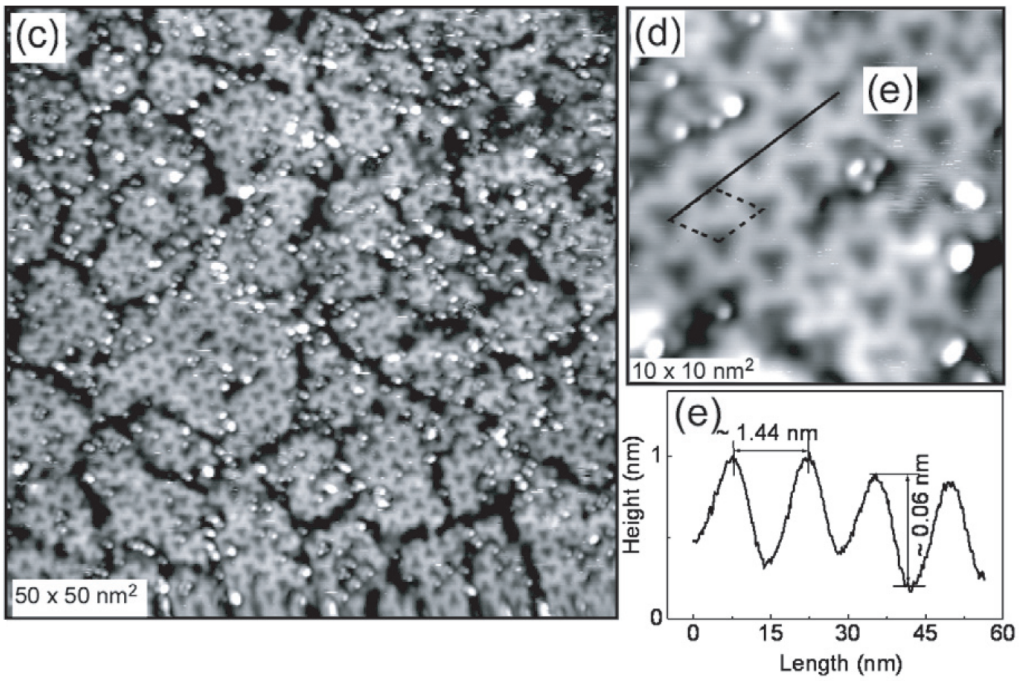

Figure 3.3: STM images of the (111) surface of Sn-doped In_2O_3 films by Morales *et al.* [26]. The surface shows similar features to the oxidized surface termination: Black triangle features with a corrugation of 60 pm and a 1.44 nm unit cell side length. The black lines running through the left image are domain boundaries.

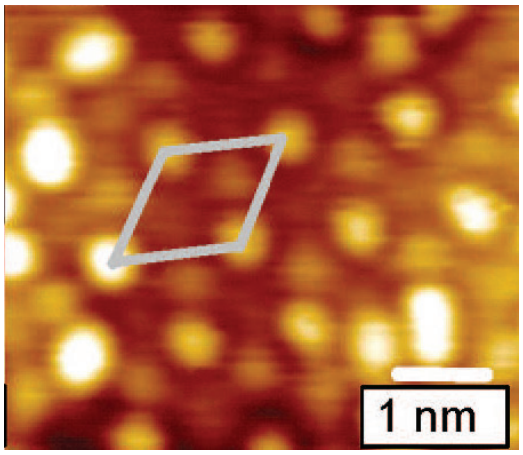

Figure 3.4: STM image of the (111) surface of an In_2O_3 film by Zhang *et al.* [27]. The surface features dots which fit the (1x1) unit cell periodicity. This unit cell is marked in the figure. The dots could correspond to the indium adatoms of the reduced surface termination. ($V_{tip} = -1.8\,V$, $I_t = 300\,pA$)

3.3 Spectroscopic Measurements of the O1s and the In3d Core Levels

Measuring the oxygen 1s core level is a standard procedure to gain information regarding the binding state of the oxygen atoms in the sample. The peaks in this region can be used to e.g. determine if OH-groups or H_2O molecules are bound to the surface. The following overview shows that the interpretation of the O1s peak in indium oxide is not completely clear.

In 1977 Fan and Goodenough [28] were the first to suggest that another type of peak could be found

Authors	Position O_{II}	Shift O_I	Shift of further peaks
Fan, Goodenough [28]	529.9 eV	+1.7 eV	non
Donley *et al.* [29]	529.5 eV	+1.1 eV	OH-groups: +2.3 eV, final state
Kim *et al.* [30]	530.2 eV	+1.3 eV	organic: +2.8 eV
Janowitz *et al.* [31]	530 eV	approx +1.9 eV	non

Table 3.1: Fitting results from various In_2O_3 and ITO publications. The positions of the peaks are given.

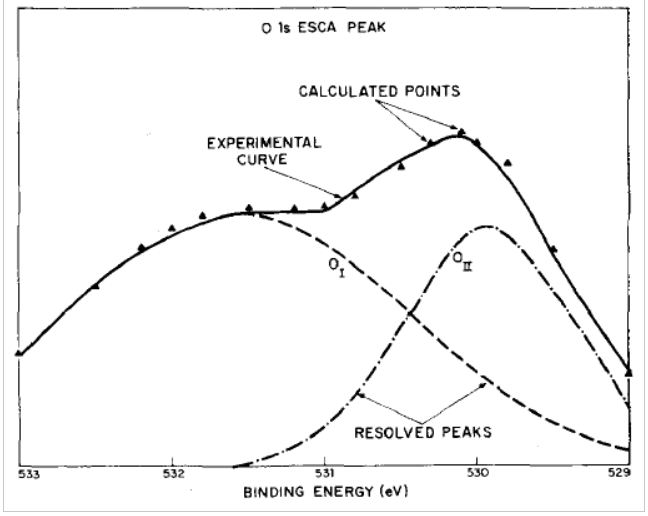

Figure 3.5: XPS measurement of the O1s peak by Fan and Goodenough [28] with two fitted subpeaks, O_I and O_{II}. The broad peak at high energies O_{II} is attributed to the oxygen vacancy sites of the reduced sample. The peak at low energies O_I is the standard In_2O_3 peak.

in the O1s region of In_2O_3: A peak resulting from oxygen vacancies (V_O). Their measurements on as-grown doped and undoped In_2O_3 films (base pressure $< 10^{-8}$ mbar) showed a very broad O1s peak that was fitted with two subpeaks, see figure 3.5. The peak at low energies (O_{II}) was identified as the standard In_2O_3 peak. The broad peak (FWHM = 2.5 eV) at high energies (O_I) was associated with oxygen near V_O sites. The paper mentioned furthermore that the O_I peak decreased when annealing in oxygen, which supported its connection to oxygen vacancies. The peak positions of all papers are given in table 3.1.

Fan and Goodenough observed that the indium 3d region did not change even in reduced samples, where a high number of oxygen vacancies were present, see figure 3.6. It was followed that the oxygen atoms surrounding an oxygen vacancy compensated its absence by donating electron density to the neighbouring indium atoms. The binding energy of the donating O atoms was shifted to higher values in the process, which resulted in the V_O peak.

Donley *et al.* [29] did similar experiments on ITO films cleaned in Triton X-100 solution in 2002. They fitted the O1s signal using 4 peaks: The O_I, O_{II}, an OH peak and a small peak to include final state effects or further contaminants, see the left panel of figure 3.7. In addition they measured an

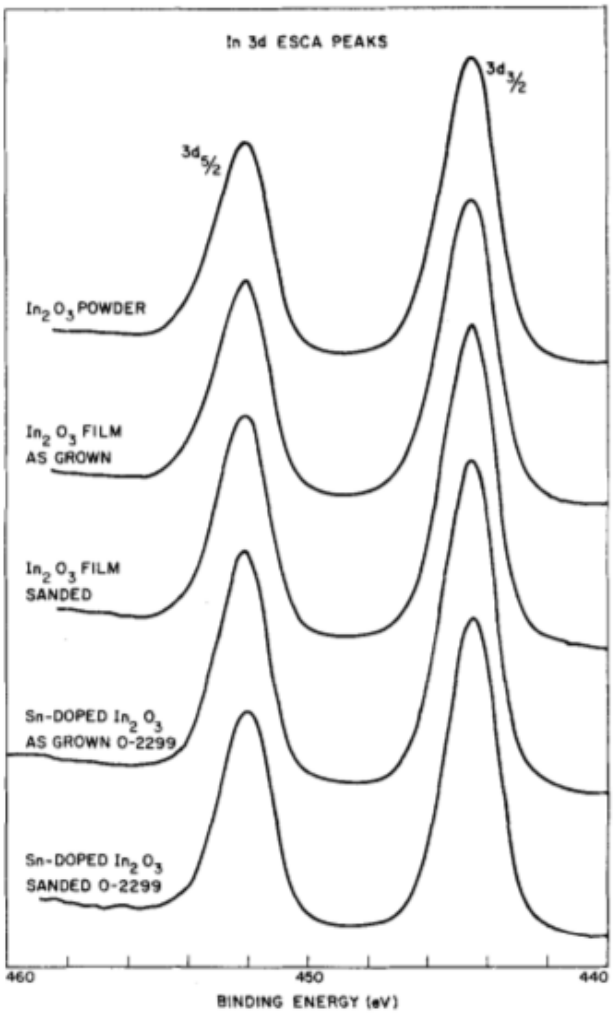

Figure 3.6: XPS measurement of the In3d region of different indium oxide samples by Fan and Goodenough [28]. The peaks show no change in the position.

undoped In_2O_3 sample which showed a main peak with a broad shoulder at the high energy flank, see the right panel of figure 3.7.

In 1999 Kim *et al.* [30] fitted the O1s region of as-received ITO films with three peaks, see figure 3.8. They attributed their middle peak to OH and O-vacancies and the highest energy peak to H_2O or organic oxygen compounds. They reported that their surface was covered with an 8-10 Å thick carbon organic contamination layer due to handling the sample in the ambient. Their base pressure was below $5 \cdot 10^{-9}$ mbar.

Janowitz *et al.* [31] also reported on V_O peaks in 2011. They measured In_2O_3 single crystals that were cleaved in UHV and saw a clear O_{II} peak at $\Delta E = 1.6\,eV$, see figure 3.9. It was deemed a result of oxygen vacancies. Moreover they saw two additional peaks in the In3d region which were not reported by other groups. These peaks was found to be surface effects when varying the photon

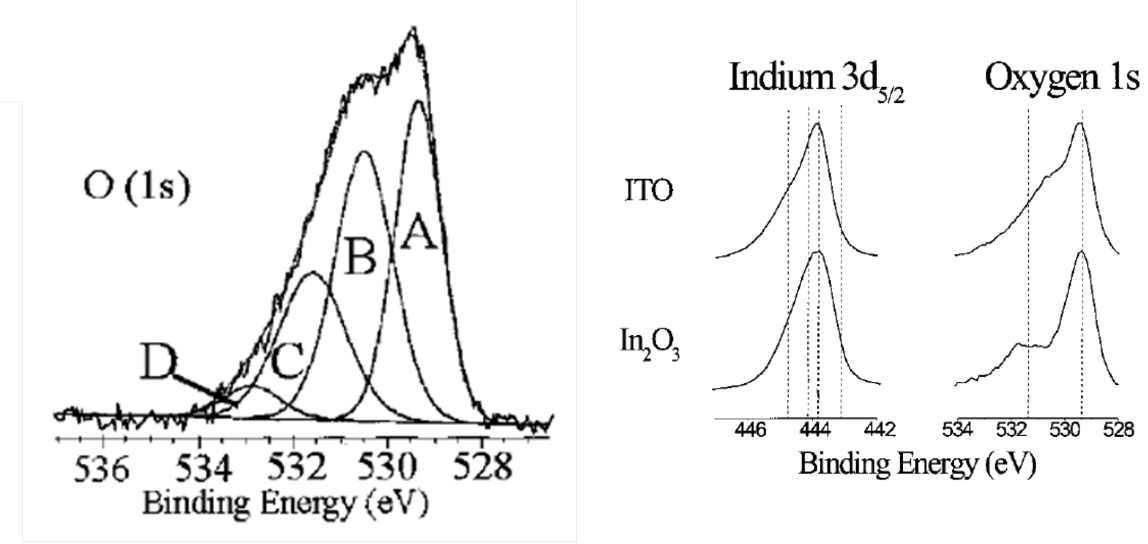

Figure 3.7: Measurements by Donley *et al.* [29]. (left) O1s XPS spectra of an ITO film, fitted with 4 peaks. Peak A is the main In_2O_3 peak. Peak B is attributed to the oxygen vacancy sites, C to OH groups and D to final state effects or contaminants. (right) O1s XPS spectra for ITO and In_2O_3 standards. Other standards are presented in the paper, but not shown here.

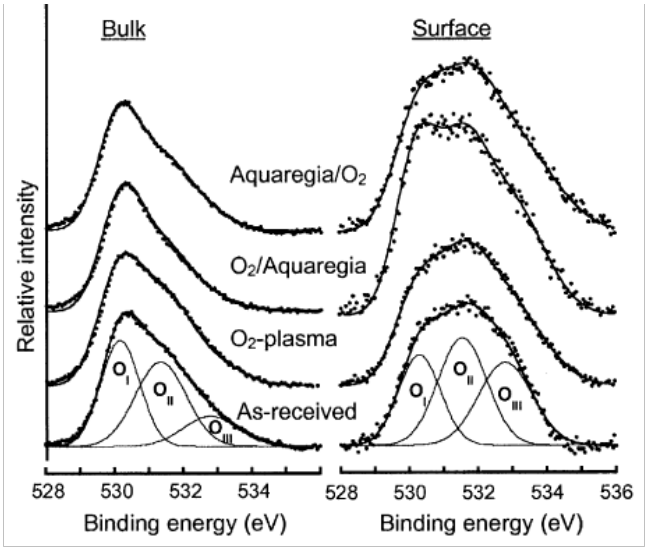

Figure 3.8: XPS measurements of the O1s region of differently prepared ITO films by Kim *et al.* [30], under different photoelectron take-off angles. (left) $\Theta = 0°$, escape depth 20 Å; (right) raised surface sensitivity with $\Theta = 80°$, escape depth 3.5 Å. The peaks are fitted with 3 components: A main peak (O_I), a peak for oxygen vacancies and OH groups (O_{II}) and a contaminant peak (O_{III})

energy from 640 eV to 1 keV. With the raised surface sensitivity, the O_{II}/O_I ration changed from 6:1 to 3:1.

Morales [32] reported on the indium 3d spectrum of indium foil in metallic, O_2-exposed and O-plasma-exposed condition, see figure 3.10. The $In3d_{5/2}$ peak was shifted from 443.6 (metallic) to 443.8 eV (O_2) and 444.1 eV (O-plasma). Plasmon loss peaks were reported in the metallic spectrum and got lower with increasing oxidation level. Commercial In_2O_3 powder was measured for comparison

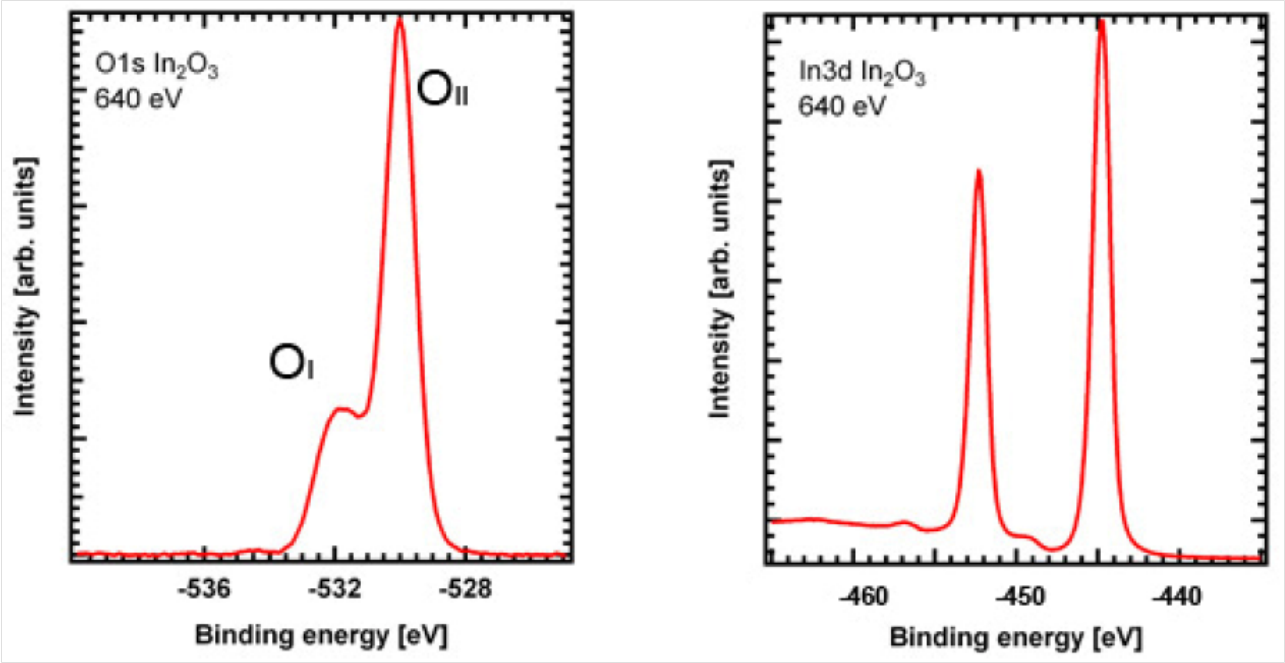

Figure 3.9: XPS measurements of the O1s (left) and In3d (right) region by Janowitz *et al.* [31]. In the oxygen region two distinct subpeaks are visible. The peak at high energies (O_I) is attributed to the reduction of the crystal. Two small additional peaks appear in the indium regions at 449 and 457 eV.

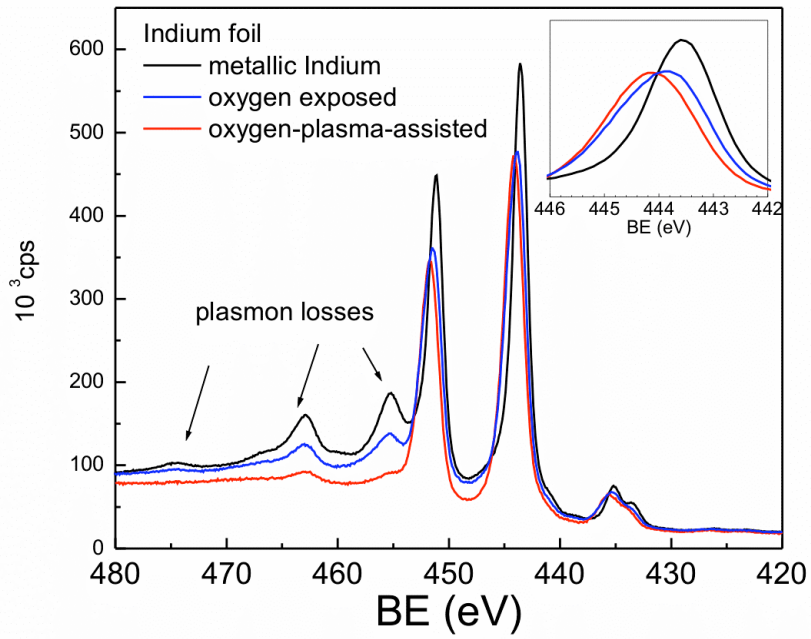

Figure 3.10: XPS measurements of the In3d region by Morales [32]. Measurements on metallic and oxidized indium foil are compared. Plasmon-loss-signals weaken with higher oxidation. The $In3d_{5/2}$ peak shifts from from 443.6 (metallic) to 443.8 eV (O_2) and 444.1 eV (O-plasma).

(not shown), where the peak was shifted to 444.2 eV.

Zhang [33] reported in detail on the differences between the $In3d_{5/2}$ peaks of undoped and Sn-

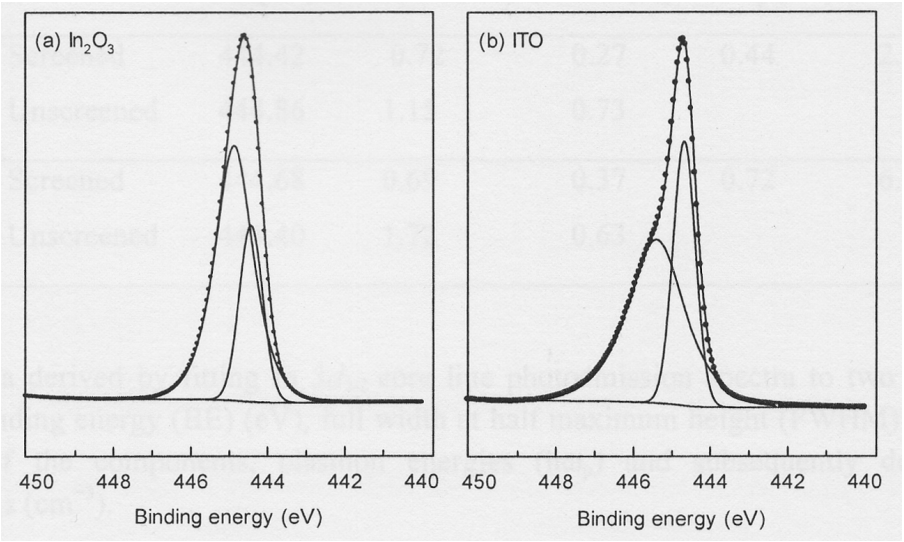

Figure 3.11: XPS Measurements of the In3d region of undoped and Sn-doped In_2O_3 by Zhang [33]. Two subpeaks are fitted, occurring due to different final states.

doped In_2O_3. The doped sample showed a significant shoulder at high energies, see figure 3.11. The changes were interpreted as final state effects. A screened and an unscreened final state are possible, depending on whether the core hole stays empty or is filled by an electron of the conduction band. The probability for the latter increases with higher carrier concentrations, i.e. higher doping levels. A similar shoulder appeared in the oxygen 1s region (not shown).

In summary an oxygen vacancy signal was reported by several groups under very different conditions and base pressures. All results are influenced by contaminants, high base pressures or in the case of Janowitz *et al.* accompanied by other unclear results. The In3d region is discussed by Fan and Goodenough [28], as well as Morales [32] and Zhang [33].

Chapter 4

Results and Discussion

4.1 Water Related Phenomena

Water vapor commonly interacts with indium oxide since it can be found both in the residual gas of vacuum chambers and in the atmosphere. Therefore the interaction between water molecules and the In_2O_3 (111) surface was investigated. The formation of OH-groups on the surface and a raised mobility of indium adatoms are reported.

4.1.1 The Oxidized Surface

After dosing 0.2 L of water the oxidized surface showed bright, triangle-shaped features in STM. Figure 4.1 shows this in two sizes. The coverage rises with rising dosage. Dosing 1.2 L creates a full monolayer, see figure 4.2. The white triangles are thermally stable: Post-annealing the sample to 100 °C does not reduce the coverage.

The white triangles form the same (1x1) structure as the dark triangles on the clean oxidized surface. They do not replace the smaller dark triangles but sit between them, see figure 4.3. They are rotated by 180 °C with respect to the dark triangles.

Whether at partial or at full coverage, the white triangle features always appear with the same height of approximately 45 pm, see figure 4.2, and are uniform in shape and appearance. They are mobile, see figure 4.4, even without tip interaction and do not jump more than one unit cell. For a statistical analysis of the hopping frequency not enough data is available. After the jump the empty surface is seemingly unchanged from the regular, oxidized surface. At low voltage biases both types of triangles are imaged in more detail and the dark triangles show a certain rotational direction, see figure 4.3, as will be discussed in section 4.1.4.

XPS and UPS measurements reveal the identity of the white triangles as OH-groups. After dosing 12.5 L of water, the O1s peak was measured with a shoulder at high energies, see figure 4.5. The additional peak is shifted by 2 eV which corresponds to OH [34]. This resembles the measurement of undoped In_2O_3 done by Donley *et al.* [29], see chapter 3.3. Figure 4.6 shows fitted[1] measurements of the oxidized surface with and without dosed water. The O1s peak was fitted using a main peak at 530 eV and an OH-peak at 531.7 eV (without dosed water) and 531.5 eV (with dosed water). The OH related peak accounts for 10% of the peak area on the surface without deliberate water dosing and about 29% after dosing 12.5 L.

The In3d peaks, see figure 4.7, showed a shift of 0.3 eV to lower binding energies after dosing 12.5 L water, while the O1s was shifted by 0.5 eV. These shifts could originate from (upward) band bending. The difference between the energy shifts of the O1s and In3d peaks can be explained with variations of the synchrotron radiation energy, i.e. the beam energy is not completely stable over the course of several hours. In the valence band two new peaks appeared at 8.8 and 10.8 eV, see figure 4.8. These are also linked to OH-groups. The interpretation of the spectra will be covered in detail in the analysis section.

4.1.2 The Reduced Surface

As mentioned in chapter 3.2, a different In_2O_3 surface termination can be prepared by annealing in UHV, which leads to single In adatoms [19]. Dosing water on this reduced surface led to disordered indium adatoms. Figure 4.9 shows an STM image of the reduced surface after dosing 2.4 L of water. The adatoms became mobile and started to agglomerate, preferably near step edges. Regions without adatoms behaved like the oxidized surface, i.e. exhibited the water-related bright triangles shown above.

When the sputtered surface is annealed in UHV and $1 \cdot 10^{-7}$ mbar O_2 are dosed while cooling from 100 to 80 °C, small indium oxide clusters and adatoms appear. Figure 4.10 shows that after dosing 16 L of water on this surface, the adatoms had moved to step edges or clusters. The clusters did not grow significantly.

[1] The fitting was conducted with CasaXPS. A linear background was used for all fits. The line shape used was an approximation of the Voigt function which is a combination of a Gaussian and Lorentzian line shape:

$$GL(x, F, E, m) = \frac{\exp(-4 \ \ln(2(1-m)\frac{(x-E)^2}{F^2}))}{1+4m\frac{(x-E)^2}{F^2}}$$

where x is the variable, F^2 the variance and E the mean value of the peak. m describes the ratio between the Gaussian and Lorentzian parts in percent, where $m = 100$ is a pure Gaussian and $m = 0$ a pure Lorentzian. Here m is set to 30.

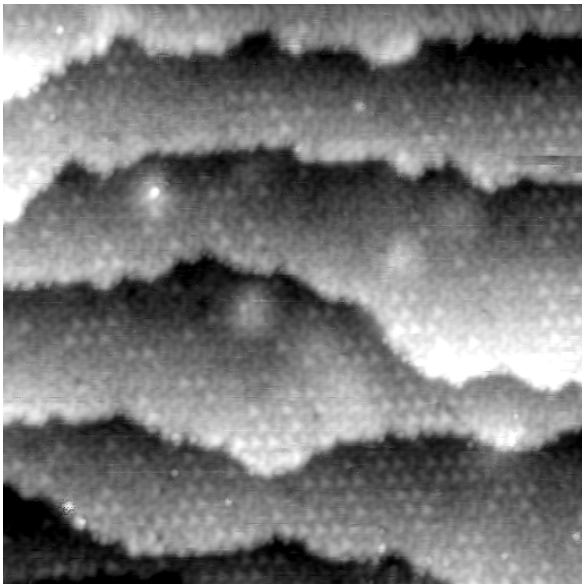

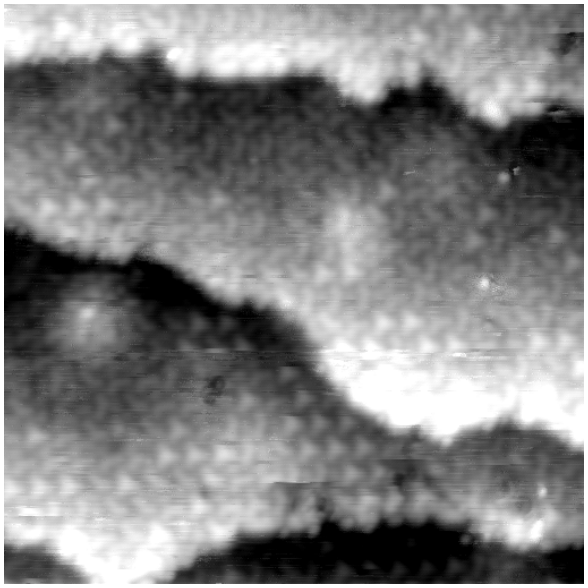

Figure 4.1: 50 x 50 nm^2, +1.9 V, 0.25 nA; data2020 30 x 30 nm^2, +1.9 V, 0.23 nA; data2021
The oxidized In_2O_3 (111) surface directly after dosing 0.2 L water at room temperature. Both dark and bright triangle features can be seen. White triangles are water related and are located between black triangles.

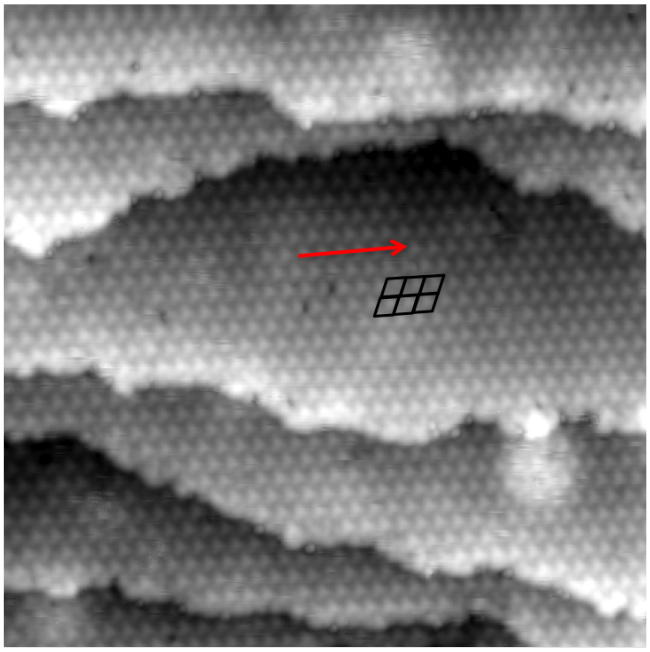

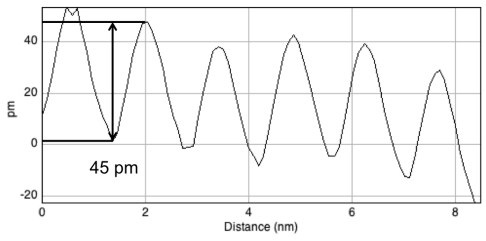

Figure 4.2: 50 x 50 nm^2, +1.4 V, 0.21 nA; data2323
The oxidized In_2O_3 (111) surface after dosing 1.2 L of water. The whole surface is covered in water related, white features. One protrusion per unit cell appears. Six unit cells are indicated in black as a reference. The arrow indicates the position of the line scan shown on the right.

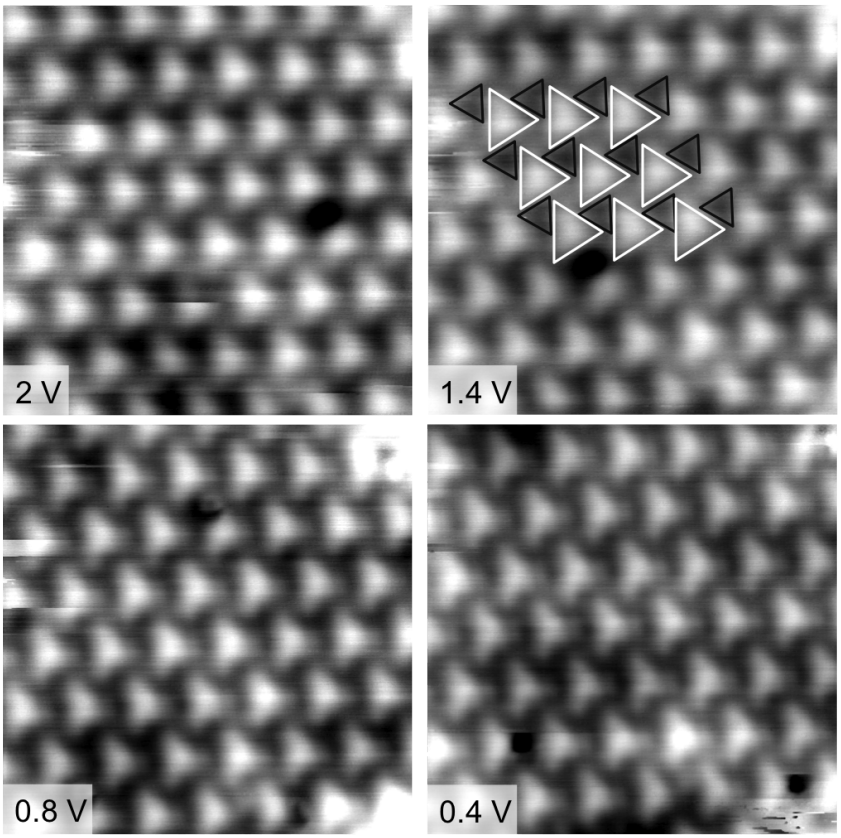

Figure 4.3: 10 x 10 nm^2, varying V, 0.14 nA; (from upper left to lower right) data2330, 2327, 2331, 2333
Consecutive STM images of water induced surface features, taken on the same are with different bias voltages. At lower voltages the rotational sense of the black triangle features can be resolved and the white triangles are imaged in more detail. In the top right figure the white and black triangle features are indicated.

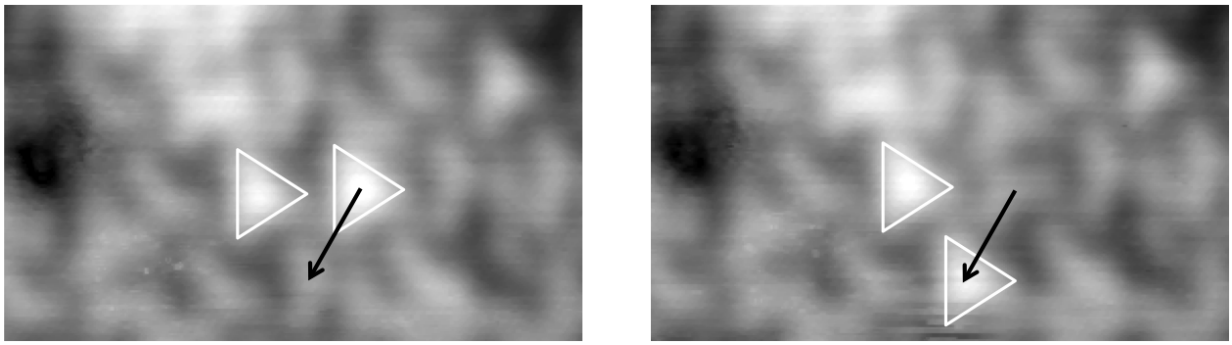

Figure 4.4: 8.3 x 4.8 nm^2, +1.1 V, 0.19 nA; data2314 (split)
The oxidized In_2O_3 (111) surface after dosing 0.1 L of water. Both dark and bright triangle features can be seen. The marked white feature jumps to a neighboring site. The now empty site is again seemingly unchanged from the regular, oxidized surface. In the top right corner a white triangle feature can be seen without a white mark.

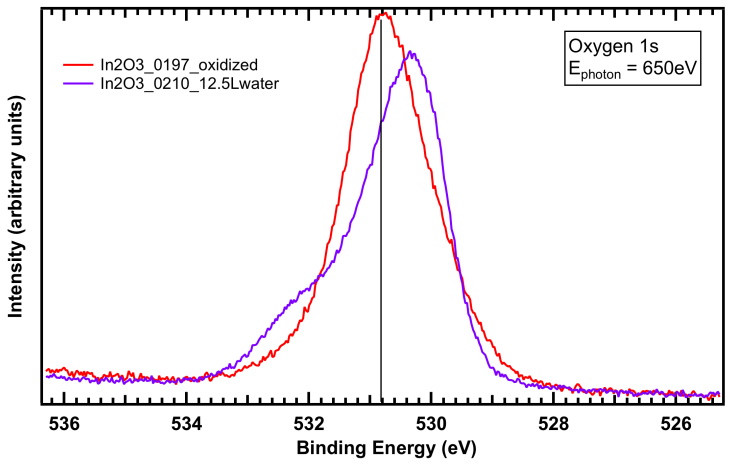

Figure 4.5: XPS measurement of the oxygen 1s peak of the oxidized In_2O_3 (111) surface with varying amounts of dosed water. At 12.5 L a shoulder appears at the high energy side of the peak. The main peak is shifted by 0.5 eV, which can be attributed to upward band bending.

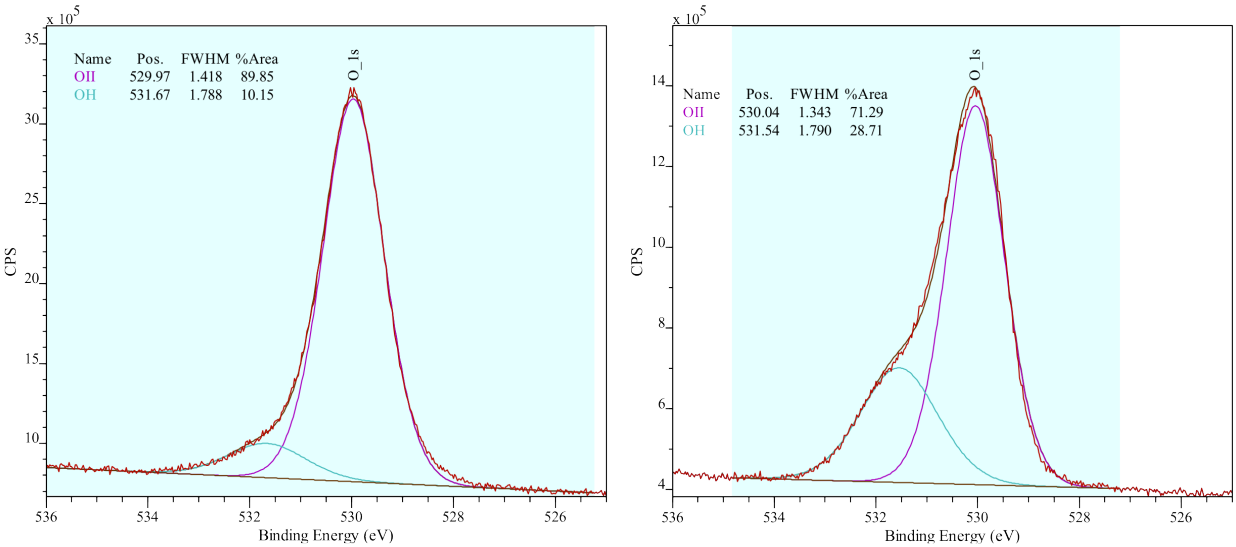

Figure 4.6: Fitted core level measurements of the O1s region of the oxidized In_2O_3 (111) surface termination without dosed water (left) and after dosing 12.5 L water (right). Each measurement is fitted with two peaks: The main peak at 530 eV and an OH peak shifted by +1.7 and +1.5 eV, respectively. The OH related peak accounts for about 10% and 29% of the peak area, respectively. The fits were performed using manual peak distances. The data was acquired with a photon energy of 650 eV at normal incidence and grazing emission (angle between surface normal and analyser: left: 55°, right: 65°). (Measurement 0284, 0210)

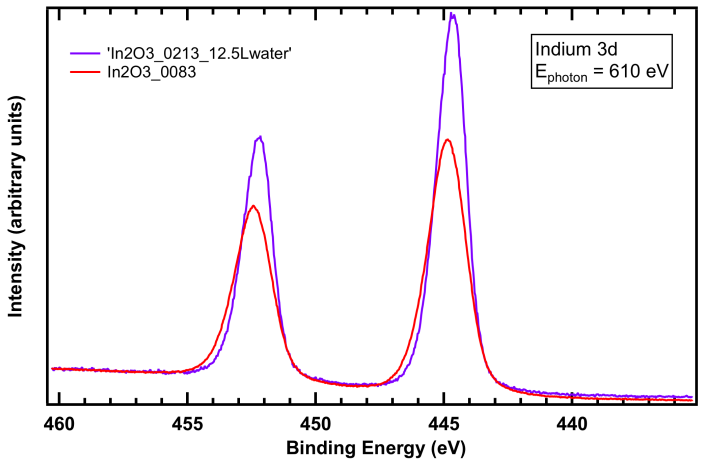

Figure 4.7: XPS measurement of the indium 3d peaks of the oxidized In_2O_3 (111) surface with and without dosed water. At 12.5 L the peaks are shifted by 0.3 eV, which can be attributed to upward band bending. The reason for the different heights of the peaks is not clear. The beam positions on the sample influences the peak height, but on average measurements after dosing water show higher indium peaks.

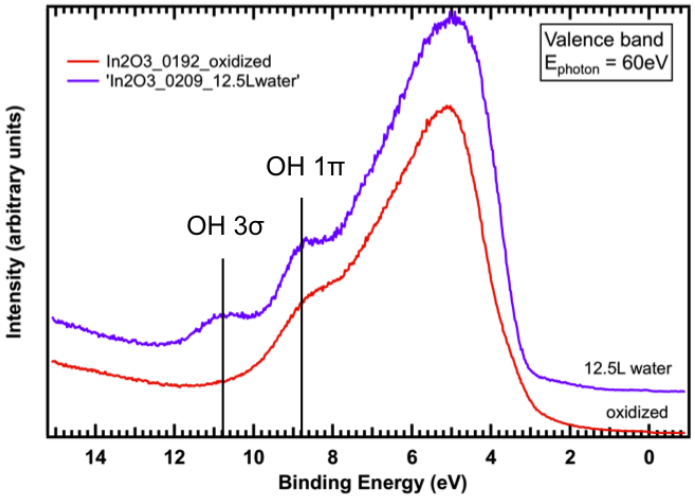

Figure 4.8: UPS measurement of the valence band of the In_2O_3 (111) surface with and without water dosed at room temperature. Two distinct peaks appear. The peak at 8.8 eV corresponds to the 1π orbital of OH, the peak at 10.8 eV to the 3σ orbital, according to [34]. The data was acquired with a photon energy of 60 eV at normal incidence and grazing emission (65°).

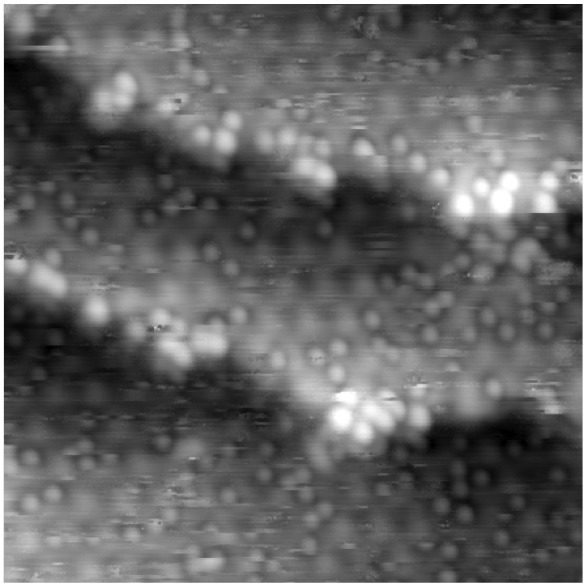

Figure 4.9: 20 x 20 nm^2, +1.4 V, 0.21 nA; data0592
The reduced In_2O_3 (111) surface plus 3 L water. Indium adatoms appear as brighter dots. They are disordered due to the interaction with water and start to agglomerate, preferably near step edges.

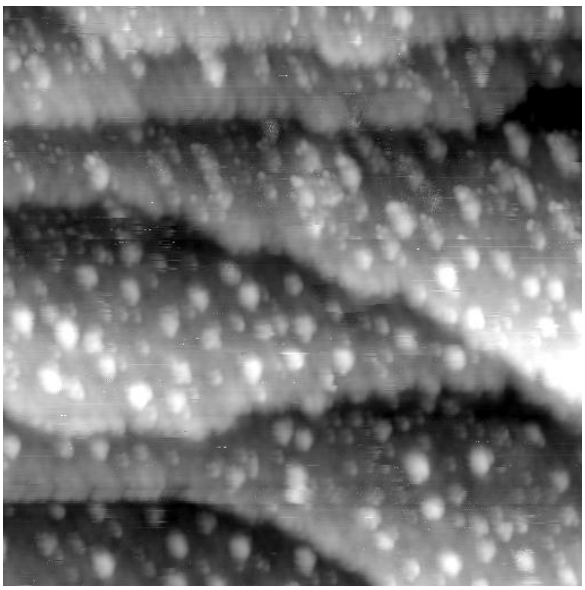

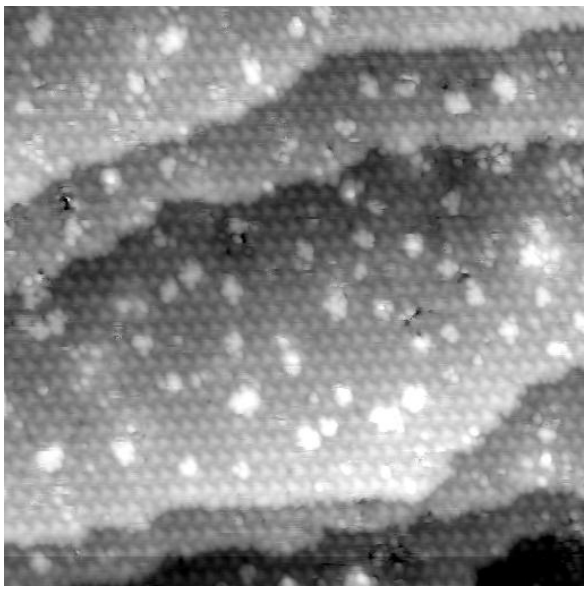

Figure 4.10: 50 x 50 nm^2, +1.7 V, 0.25 nA; data1956 50 x 50 nm^2, +2.2 V, 0.21 nA; data1979
An In_2O_3 (111) surface covered with indium oxide clusters (left, imaged with double tip) and adatoms was prepared, as described in the text. After dosing 16 L of H_2O (right) the clusters were stable. The adatoms moved to step edges or clusters. The surface between the clusters showed white triangle features induced by the water.

4.1.3 Observed STM Features

Figure 4.11 shows an oxidized surface exposed to 0.2 L of water in the upper part. The lower part shows a partially reduced surface without water. All surface features are marked:

- Circled in black are normal, unoccupied unit cells of the oxidized surface. As is explained in chapter 3.2, the dark triangles result from the sixfold-coordinated indium atoms sitting at the four corners of the unit cell.
- Circled in red are water related white triangles. These features are situated between the dark triangles and have an apparent height of 45 pm.
- Highlighted in orange are dark features which deviate from the triangle shape. One special type is circled in violet: Dark unit cells with an additional small protrusion. These could originate from a defect such as a flipped atomic bond or an impurity.
- A cluster is marked in blue.
- Normal indium adatoms are circled in green. They appear 120 pm high.

4.1.4 Analysis

4.1.4.1 The Oxidized Surface

XPS and UPS measurements show peaks originating from OH-groups. In XPS the oxygen 1s peak shows a shoulder between 531.5 and 531.7 eV. In contrast to OH, the O1s peak of molecular water is typically found between 533-535 eV, see table 2 in [35].

XPS measurements conducted on the oxidized surface show a small OH-peak. This peak results from residual water in the chamber and fills 10% of the peak area. After dosing 12.5 L of water, the peak area rises to 29%. One H_2O molecule interacting with the surface creates 2 OH groups:

$$H_2O + O_{\text{surface}} \Rightarrow 2OH$$

Assuming the simplified picture that only the first layer of O atoms (24) contributes to the signal, one H_2O molecule per unit cell would result in a ratio between OH and surface oxygen of 2/22, or 9.1%. This is roughly the ratio we observe in XPS. The coverage after deliberate water dosing (29% peak area) results from 6 OH-groups per unit cell.

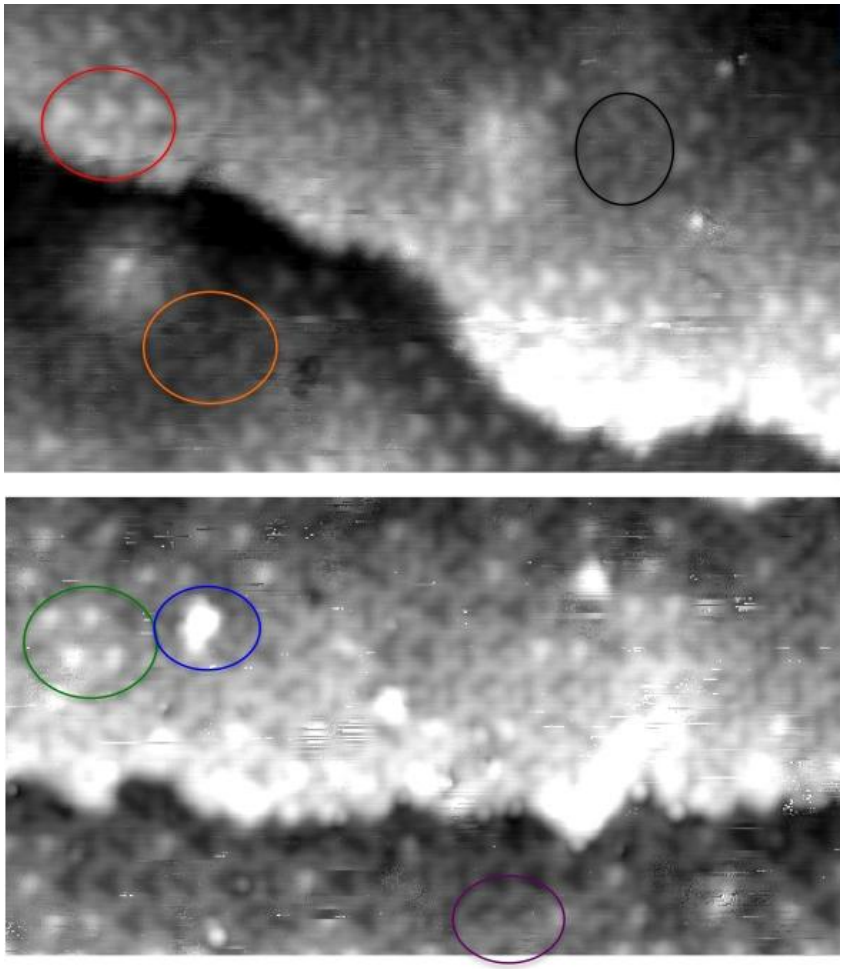

Figure 4.11: 17 x 30 nm^2, +1.9 V, 0.23 nA; upper: data2021, lower: data2044
Two images of different surface preparations showing all surface features that can be observed when dosing water on the In_2O_3 (111) surface. The top figure shows the oxidized surface exposed to 0.2 L of water. The lower figure shows a partially reduced surface.

The UPS measurements show two new peaks in the valence band as is expected for OH. The peak at 8.8 eV is attributed to the 1π orbital, the peak at 10.8 eV to the 3σ. The typical binding energies of OH on metals are lower, 5-7 eV and 9-11 eV, respectively [34]. H_2O would result in three peaks [35].

The location of the OH-groups can be narrowed down by mapping STM images to the surface model using the dark triangle features. Both their direction and their sense of rotation must fit the model.

The sense of rotation of the dark triangle is created by the six oxygen atoms that surround the inner sixfold-coordinated indium atom. Unpublished DFT calculations by Bernd Mayer and Steffen Seiler, Friedrich-Alexander-Universität Erlangen-Nürnberg, show that the threefold-coordinated oxygen atoms appear bright and the fourfold-coordinated O atoms are barely visible. As the positions of the bright oxygen atoms are shifted clockwise in regard to the (dark appearing) indium atoms, an

rotational direction can be observed.

Figure 4.13 shows how the surface model can be overlapped with STM data. Both the orientation and the rotational direction fit. This overlap shows that the OH-group (white triangle feature) is always centered to the ring at site A. This ring consists of three fivefold-coordinated indium atoms and three threefold-coordinated oxygen atoms. Ring C, which is similar but consists of three fourfold-coordinated O atoms, appears dark on STM images. The lower coordination explains why OH-groups bind to ring A, since the oxygen atoms there have dangling bonds that wish to bond to other atoms.

In our STM measurements, all white triangles appear in the same brightness and form. A site with two or more OH-groups is expected to appear brighter than a site with one OH-group. However we observe no variations. Furthermore, when the white features move, the whole feature moves and the oxidized surface appears at the old site. It would therefore be conclusive if only one OH-group could be situated at one ring site. This contradicts XPS results, where 2 OH-groups per unit cell are measured. In this case one white triangle would contain 2 OH-groups which jump together. The higher coverage of 6 OH-groups can not be observed in STM.

The OH triangles are bigger than the dark triangles on the oxidized surface. One or two OH-groups could result in a feature of that size by moving between various adsorption sites. These sites would have to feature similar binding energies. Further theoretical calculations are needed to shed light on the preferred adsorption sites of the OH group.

4.1.4.2 The Reduced Surface

The raised mobility of the indium adatoms results from new bonds to atoms of the water molecule. They weaken the bonds to surface oxygen atoms and lead to a more frequent hopping between sites. Clustering and sites near step edges are energetically preferable. These positions are assumed as a result of the raised mobility.

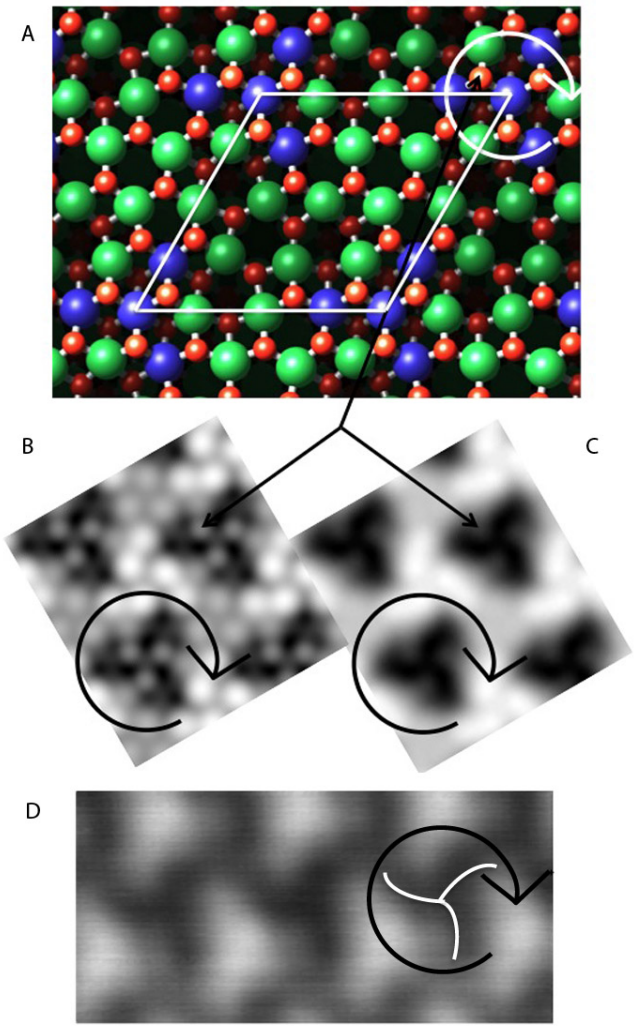

Figure 4.12: The rotational direction of the dark triangle features visible in STM images (D) can be understood when looking at theoretical DFT images (B/C) and the surface model (A). The same threefold-coordinated oxygen atom is marked in A-C by black arrows. It appears bright and leads to the screw shape visible in the panels C and D since it is situated slightly off the axis between the indium atoms.
STM image (D): 2 x 5 nm^2, +0.4 V, 0.14 nA; data2333; Simulated STM images were calculated using a voltage of +1.4 V and an iso-density of $1.6 \cdot 10^{-5}$ e/$bohr^3$ (B) or $1 \cdot 10^{-6}$ e/$bohr^3$ (C)

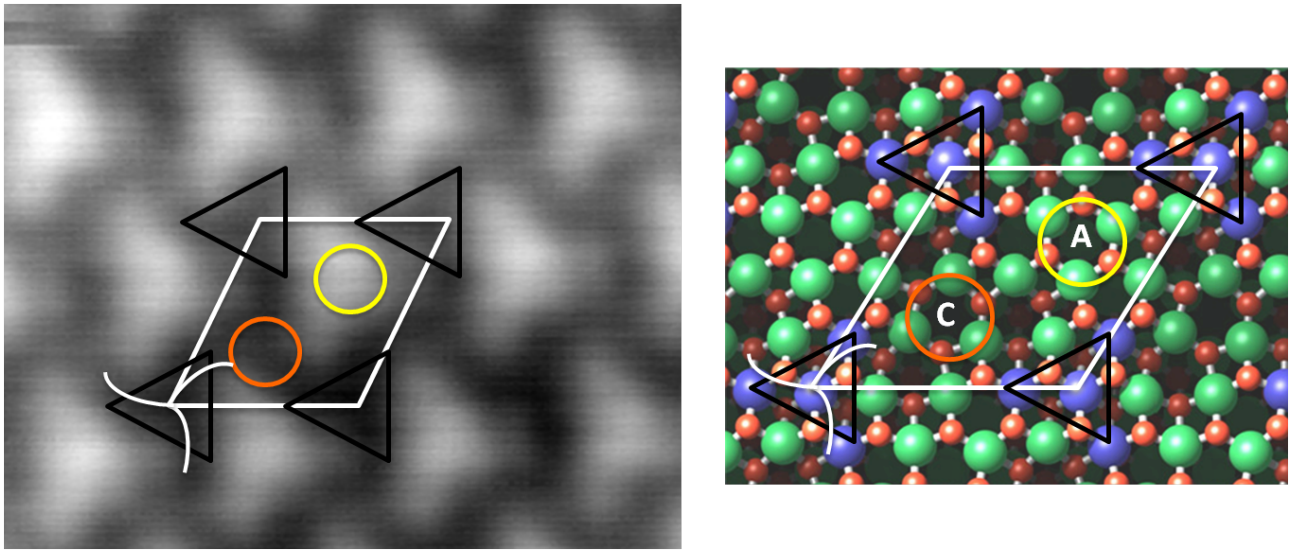

Figure 4.13: 4 x 6 nm^2, +0.4 V, 0.14 nA; data2333
Comparing the surface structure model with an STM image shows that the center of the white triangles is located at site A. This is a ring of three fivefold-coordinated indium atoms and three threefold-coordinated oxygen atoms. Site C on the other hand seems to be strongly disfavored by OH-groups. The unit cell and the black triangles are marked in white and black, respectively, in both figures. The rotational direction is indicated in white. Observe the threefold coordinated oxygen atoms which are the reason for this rotation.

4.2 Effects of Crystal Reduction

Fan and Goodenough wrote in their 1977 paper [28] that oxygen vacancies were the reason for an additional component in the oxygen 1s peak, see chapter 3.3. Our crystal (number 1, see chapter 2.4.1) was measured two times, in 2013 and in 2014, using XPS at the synchrotron in Lund, Sweden. During the year between the measurements the crystal was visibly reduced by repeated sputtering and annealing processes. Its color changed from bright yellow (as can be seen in figure 2.3, chapter 2.4.1) to a slight red. This reduction should result in a higher concentration of oxygen vacancies. The crystal could therefore be the ideal test system to find a peak resulting from oxygen vacancies.

4.2.1 Measurement Results

The oxidized surface termination was measured in 2013 and with a visibly more reduced crystal in 2014, see figure 4.14. The left panel shows the O1s region from 2013 which featured a main peak at circa 530 eV with a shoulder at high energies. The shoulder was fitted with a subpeak shifted by ΔE = +1.7 eV, which is attributed to OH-groups on the surface, as explained in the previous chapter. The right panel shows the same measurement repeated in 2014. The O1s region could also be fitted with a main peak and a subpeak. The main peak at 530.3 eV was broader, the FWHM increased from 1.42 to 1.55 eV. The shoulder was shifted by ΔE = +1.3 eV.

The same effect was observed in the In3d region of the oxidized In_2O_3 (111) surface. Figure 4.15 shows that the In peaks were broader in the 2014 measurements.

4.2.2 Analysis

An additional O1s peak resulting from oxygen vacancies, as described by Fan and Goodenough [28], can not be confirmed by the measurements presented above. Although our crystal was visibly more reduced in the second set of measurements, no additional peak is observed. The increase in peak broadness of the O1s and In3d peaks is explained by Zhang [33], see chapter 3.3. He describes that the In3d peak consists of two peaks in close proximity resulting from two final states. A raised conductivity (through a higher reduction) leads to a different probability of final states and therefore to a different ratio between the two peaks and an increase in peak broadness.

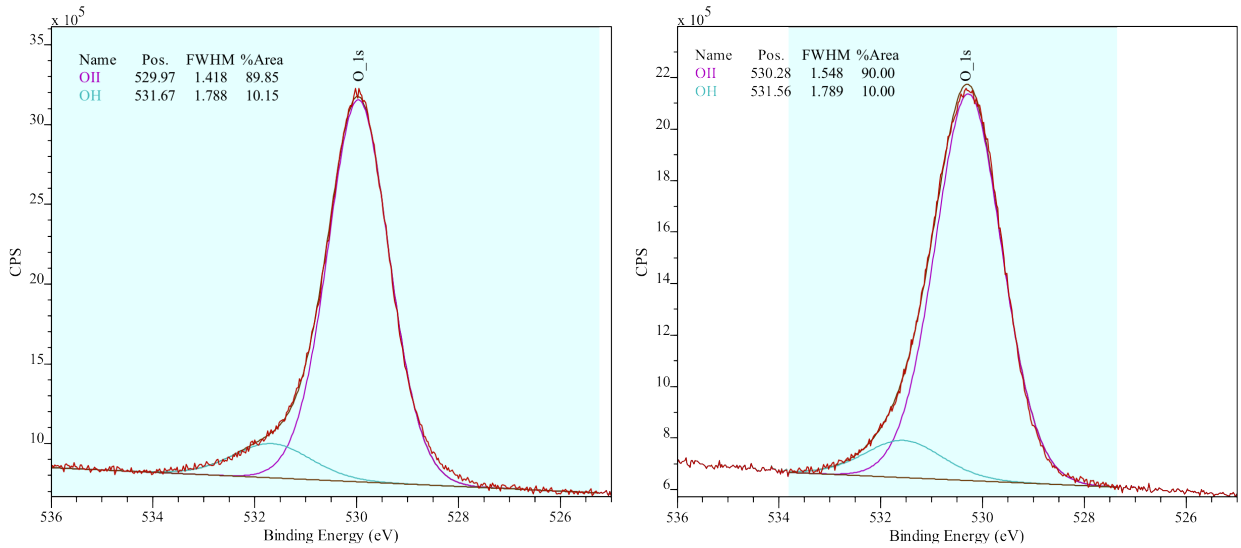

Figure 4.14: Core level measurements of the O1s region of the oxidized In_2O_3 (111) surface termination from 2013 (left) and 2014 on a visibly more reduced crystal (2014). Each measurement is fitted with two peaks. The OH related peaks account for about 10% of the peak area. The fits were performed using (left) a manual peak distance and (right) using a manual peak area ration. The data was acquired with a photon energy of 650 eV at normal incidence and grazing emission (left - 55°, right - 65°). (Measurement 0284, 0298)

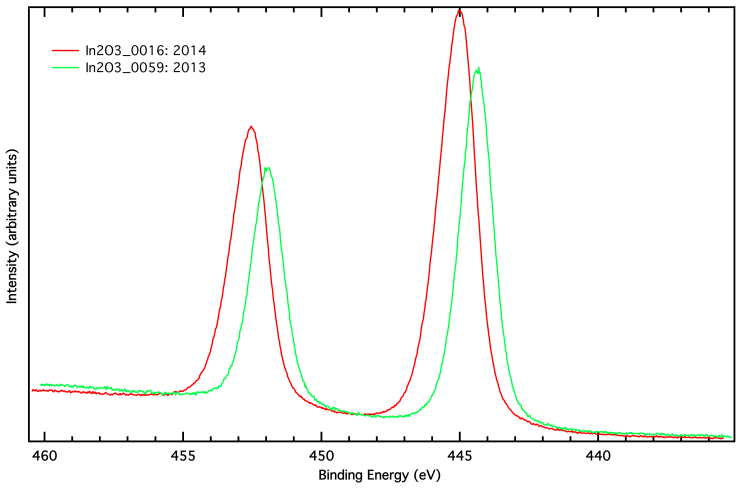

Figure 4.15: Core level measurements of the In3d region of the oxidized In_2O_3 (111) surface termination from 2013 (green) and 2014 (red). The FWHM of the $In3d_{3/2}$ peak changed from = 1.35 eV (2013) to 1.53 eV (2014). The data was acquired with a photon energy of 550 eV (2013) and 610 eV (2014) at normal incidence and grazing emission (55° (2013), 65° (2014)).

4.2.3 Discussion

Fan and Goodenough [28], Kim *et al.* [30], Donley *et al.* [29] and Janowitz *et al.* [31] report on an additional peak in the O1s region resulting from oxygen vacancies (V_O), see chapter 3.3. The theory of Fan and Goodenough describes that O atoms near V_O give electron density to neighbouring In atoms. As a result the binding energy for the electrons remaining at the O atoms increases, while the In oxidation state does not change.

Fan and Goodenough report that the binding energies of the peaks in the In3d region of doped and undoped In_2O_3 are the same. They follow that all In atoms have the same oxidation state, In^{3+}, and therefore build the above theory to explain this effect.

The work of Morales [32] investigates the change of the In3d region in detail. The shift between metallic In and In_2O_3 is 0.6 eV. It is therefore not surprising that Fan and Goodenough could not resolve the differences between oxidation states due to their high FWHM of 2.5 eV.

Fan and Goodenough and Kim *et al.* measured on unclean samples. Kim *et al.* mention a 8-10 Å carbonate sheet covering their thin film. The resulting peaks at high energies from both OH-groups and other contaminants makes a further analysis difficult. Fan and Goodenough measured in a base pressure of $1 \cdot 10^{-8}$ mbar.

Donley *et al.* measured the O1s core level which clearly shows an additional peak at $\Delta E = +1.1$ eV. The authors explain this peak with the V_O theory of Fan and Goodenough. Zhang [33] shows that this peak results from final state effects, which can also be observed in our measurements in the previous section. The peak height difference between Donley *et al.* and Zhang is explained by the different Sn doping level: 10% and 2.2%, respectively.

The results of Janowitz *et al.* are mysterious. The O1s shoulder could originate from OH-groups, since they do not mention the base pressure. Their In3d region shows two additional peaks which can not be confirmed with the measurements in this thesis, see figure 4.15. The authors claim that this result is found due to their high surface sensitivity at photon energies of 640 eV. However the In measurements in figure 4.15 were measured with a similar photon energy of 610 eV where no additional peaks are observed. The additional peaks of Janowitz *et al.* have similarities with the plasmon-loss-peaks reported by Morales, see chapter 3.3.

In summary it can be said that the additional reported O1s peaks result from OH-groups or other contaminants or from final state effects. An increasing conductivity, through doping or oxygen vacancies, is the reason for these final state effects.

4.3 Iron Deposition

The reduced In_2O_3 (111) surface forms a well ordered (1x1) superstructure of indium adatoms, see chapter 3.2. It was investigated if a similar array of single adatoms could be created by evaporating iron on the oxidized In_2O_3 (111) surface.

Iron was evaporated at room temperature with flux rates between 0.5 and 2 monolayers per minute. As a reminder, one monolayer in this context means one adatom per unit cell, which in turn consists of 24 oxygen atoms and 16 indium atoms in the first layer.

STM measurements showed that single adatoms were formed when depositing coverages below one monolayer. The ordering depended on the coverage and could be increased by annealing. While presence of iron on the surface was shown with XPS, AES and LEIS measurements, the measurements were not conclusive as to whether the adatoms are indeed iron or possibly iron-induced indium adatoms.

4.3.1 STM Results

STM measurements showed that the evaporation of iron led to the formation of adatoms. The ordering of the adatoms depended on the amount of deposited iron. Three regimes were encountered:

- The ordered regime up to 0.6 monolayers (3 adatoms per 5 unit cells) and below. At these coverages the adatoms formed ordered arrays, see figure 4.16. The adatoms were situated in the same adsorption site as the indium adatoms of the reduced surface. Both were located in the center of the dark triangle feature formed by four sixfold-coordinated indium atoms.

- The disordered regime from 0.6 ML to approximately 2 ML. At these coverages the adatoms were not completely ordered, see figure 4.17. There were disordered, ordered, and empty regions without adatoms.

- The cluster regime above approximately 2 monolayers of iron. Figure 4.18 shows that small agglomerations as well as adatoms are present at 2.3 ML. At 38.5 ML the surface was entirely covered by clusters. The coverage was too high to measure the cluster height, as the tip could not reach the surface. At this coverage the steps were not visible anymore.

An Fe coverage of 0.7 ML was evaporated on the oxidized In_2O_3 (111) surface and was then annealed at 150 °C, 250 °C, 350 °C and 425 °C for five minutes each, see figure 4.19. The STM measurements showed that annealing at 150 °C resulted in an increase in ordering, but agglomerations were still

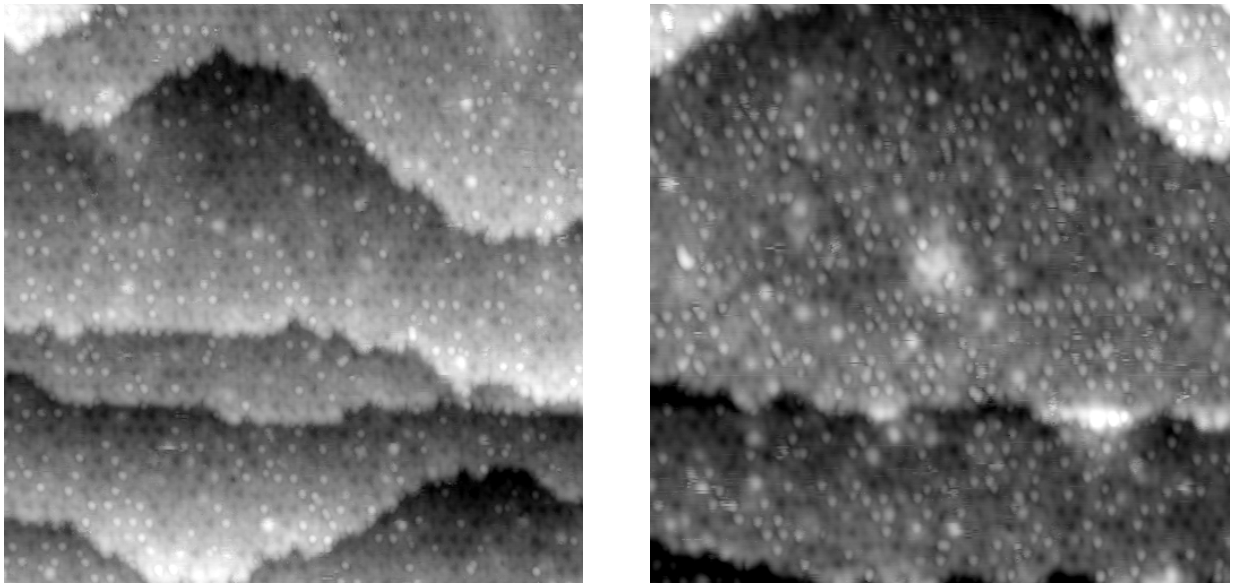

Figure 4.16: 50 x 50 nm^2, +2.2 V, 0.17 nA; data2229 50 x 50 nm^2, +1.4 V, 0.10 nA; data2166
The oxidized In_2O_3 (111) surface after evaporation of 0.28 ML (left) and 0.5 ML (right) of iron. The adatoms sit in dark triangle sites and form well ordered rows, similar to indium adatoms. The surface areas without adatoms show no change. (The wide bright region in the center of the right image is normal for the oxidized surface and could result either from impurities or Ar bubbles.)

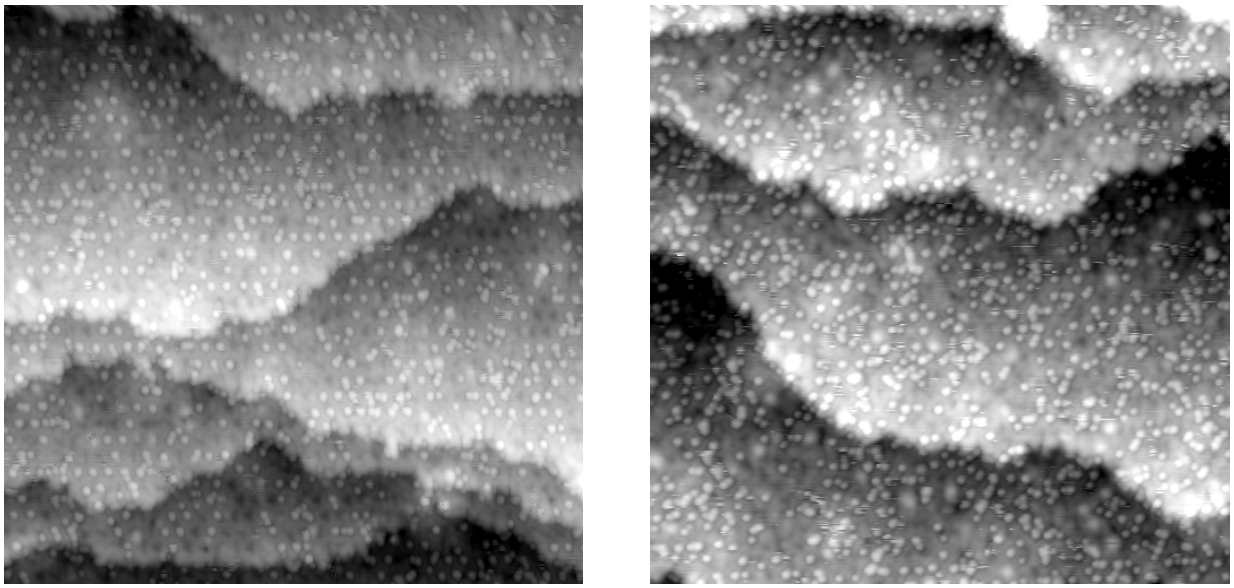

Figure 4.17: 50 x 50 nm^2, +1.7 V, 0.17 nA; data2259 50 x 50 nm^2, +1.1 V, 0.10 nA; data2179
The oxidized In_2O_3 (111) surface after evaporation of 0.74 ML and 0.81 ML of iron, respectively. Areas of ordered and disordered adatoms can be found, as well as areas without any adatoms.

visible. Annealing at 250 °C and higher resulted in a completely ordered array of adatoms. The coverage was still at 0.7 ML after annealing at 425 °C. A 10 x 10 nm^2 STM image after annealing at 425 °C is shown in figure 4.20.

The apparent height of the adatoms was approximately 100 pm and the FWHM was 0.6 nm, see figure 4.21. Indium adatoms were measured with similar values (apparent height 120 pm, FWHM

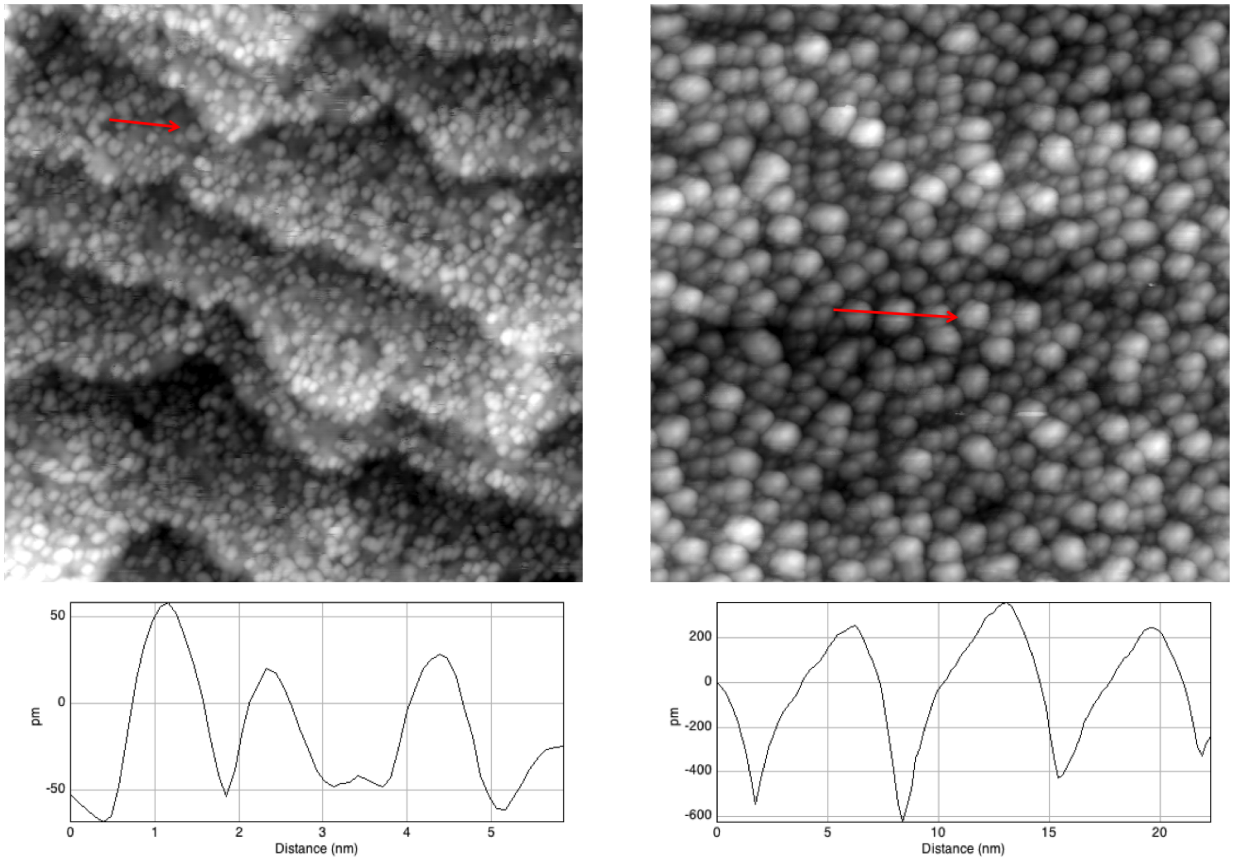

Figure 4.18: 50x50 nm^2, +1.1 V, 0.14 nA; data2137 100 x 100 nm^2, +1.9 V, 0.20 nA; data2135
The oxidized In_2O_3 surface after evaporation of more than one monolayer of iron. At 2.3 ML (left) clusters and adatoms can be seen. The line profile shows an apparent height of around 100 pm, which correspond to adatoms. The step edges are visible. At 38.5 ML (right) the surface is covered with clusters with an apparent height of more than 600 pm. The step edges of the In_2O_3 (111) surface cannot be seen anymore. Note the different scale of the right image (100 x 100 nm^2).

0.7 nm), see chapter 3.2. For direct comparison, a partially reduced surface was prepared by annealing in $1.5 \cdot 10^{-8}$ mbar O_2. After checking the amount of indium adatoms, the same amount of iron adatoms (0.27 ML) was evaporated on the surface. Even with different STM biases (+2 V to -1.8V, see figure 4.22) no differences between the adatoms could be resolved.

4.3.2 Spectroscopy

The oxidized In_2O_3 (111) surface with different coverages of Fe was investigated with XPS, using Mg Kα radiation, see figure 4.23. At a coverage of 1 ML small iron peaks appeared at 710.5 eV and 723.3 eV. The measured area was bigger than the sample surface, so a tantalum signal of the sample plate and the sample holders was measured as well.

Further XPS measurements were done at the Max-Lab synchrotron facility in Lund. The iron peaks (710.2, 723.7 eV) were visible already at a coverage of 0.5 ML, see figure 4.24. At higher coverages

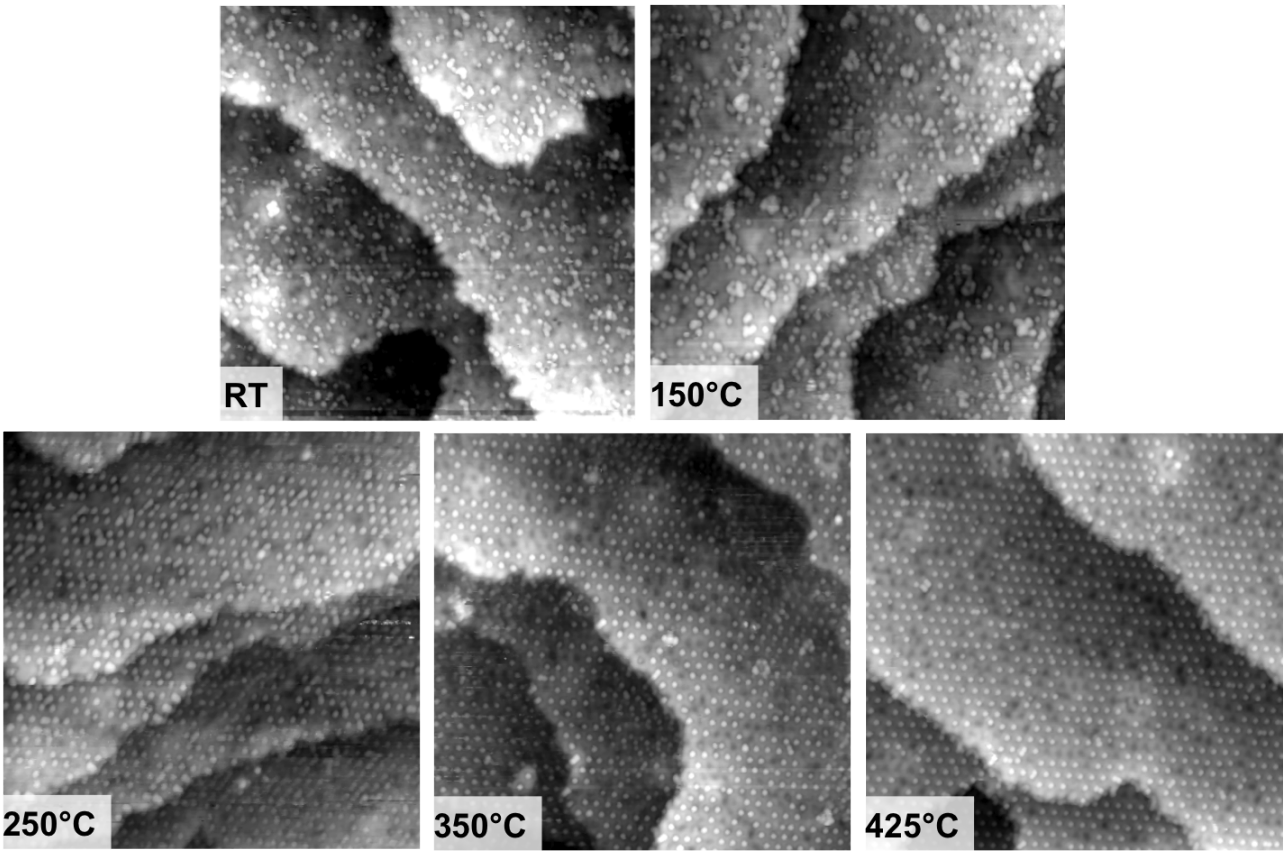

Figure 4.19: 50 x 50 nm^2, +1.7 to +2.0 V, 0.10-0.25 nA; from upper left to lower right: data0041, 0050, 0053, 0073, 0092
The oxidized surface covered with 0.7 ML of iron adatoms. Starting from the upper left, which shows the surface after the evaporation at room temperature, the sample was successively annealed at varying temperatures for five minutes each. After annealing at 150 °C the adatoms already show an increased ordering. Above 250 °C the adatoms are completely ordered. Heating above 250 °C does not seem to result in further changes. At 425 °C the coverage is still 0.7 ML.

a metallic shoulder appeared at approximately 709 eV. This shoulder can be attributed to Fe^{2+}, see [36]. At 716 eV a peak appears at higher coverages, which is also typical for Fe^{2+}. The $Fe2p_{3/2}$ peak corresponds to Fe^{3+} or a mixture of Fe^{2+} and Fe^{3+}. The examined area at the synchrotron was smaller than in the lab, yet due to the smaller crystal used for these measurements a small Ta peak was still visible.

The valence band was investigated with a synchrotron radiation energy of 85 eV, see figure 4.25. The iron evaporation led to a new peak at 2 eV.

Peak shifts were observed in both synchrotron measurements. The $In3p_{1/2}$ peak in figure 4.24 and the main VB peak in figure 4.25 were shifted to higher binding energies with increasing coverage. At 2.5 ML of Fe the peaks were shifted by 0.5 eV. These shifts could originate from (downward) band bending.

An oxidized surface with 2.4 ML iron was measured with AES, see figure 4.26. The measurement

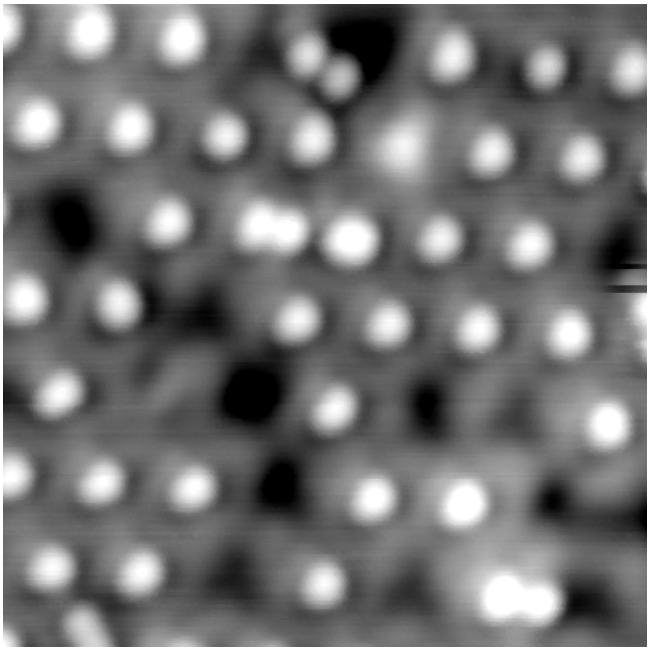

Figure 4.20: 10 x 10 nm^2, +2.0 V, 0.22 nA; data0089
The oxidized surface covered with 0.7 ML of iron adatoms after annealing for five minutes at 150, 250, 350 and 425 °C. Empty, dark triangle features of the oxidized surface and single adatoms can be seen. The adatoms also form dimers.

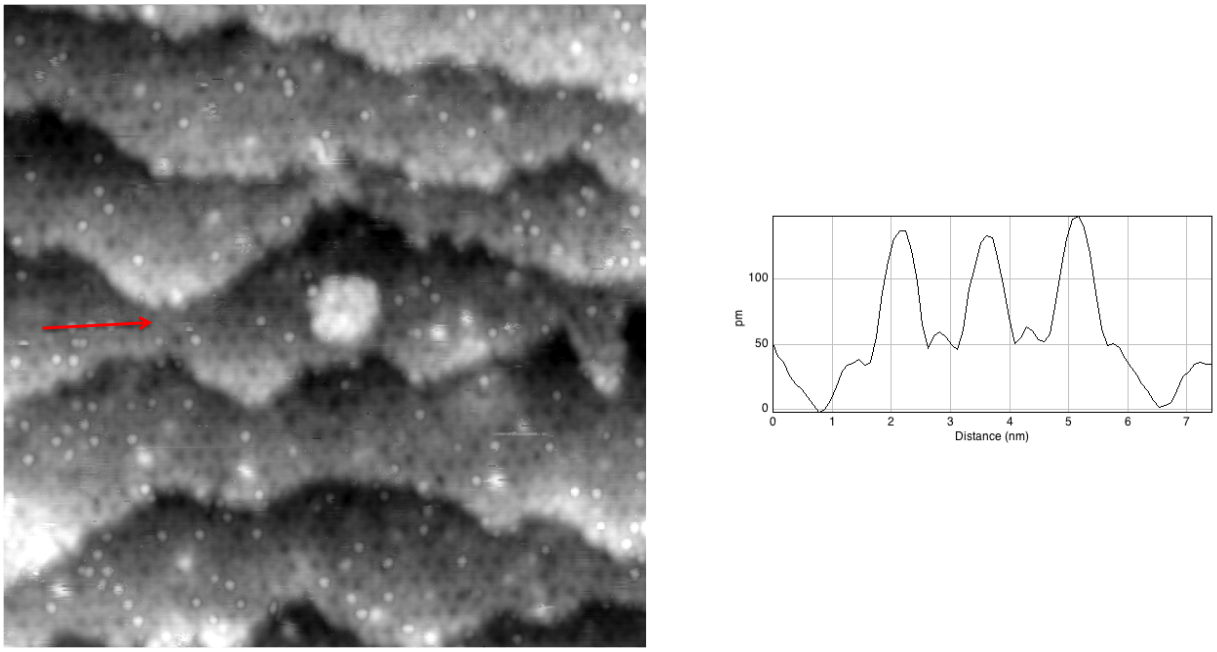

Figure 4.21: 50 x 50 nm^2, +2.0 V, 0.17 nA; data2146
The oxidized In_2O_3 (111) surface after evaporation of 0.26 ML of iron. The adatoms sit in dark triangle sites. The line profile shows an apparent height of approximately 100 pm, which is similar to the apparent height of indium adatoms.

showed oxygen, indium and iron. No Ta was visible due to the small size of the electron beam used in AES.

A LEIS measurement showed oxygen, indium and iron. Figure 4.27 shows the five runs of this

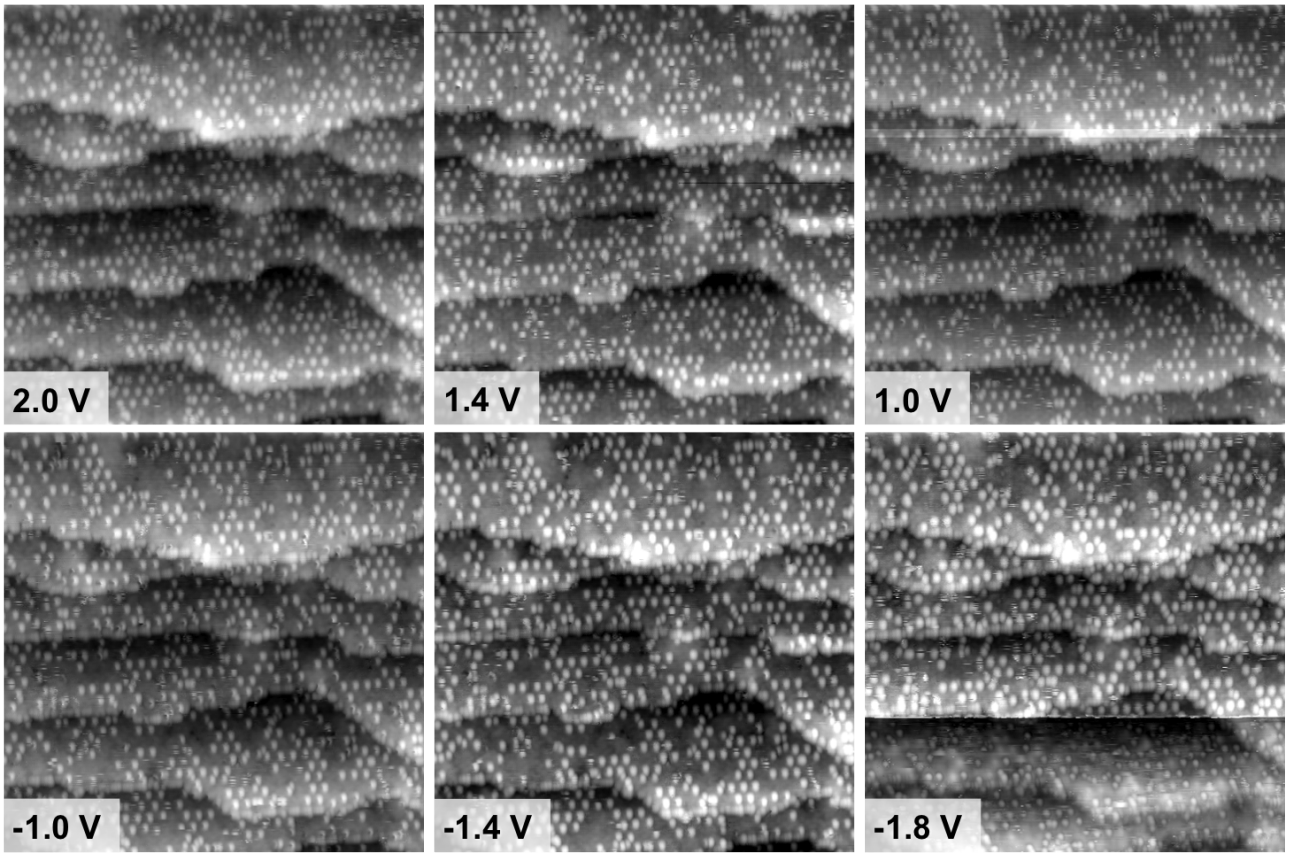

Figure 4.22: 50 x 50 nm^2, varying voltages, 0.20 nA
From upper left to lower right: data2383, 2379, 2380, 2384, 2385, 2386
A partially reduced surface covered with indium adatoms and the same amount of iron adatoms (0.27 ML) imaged with varying STM bias. No differences between adatoms is apparent that could help distinguish between In and Fe. In the lower part of the image at -1.8 V the tip condition changed.

measurement. The sputtering of the He ions removed a portion of the topmost atoms during every run. As can be seen in figure 4.27 on the left side, the iron signal weakened and was gone after the third run. The indium signal grew stronger. Note that both figures show the same measurement, but the spectra are shifted in a different way to emphasize the changes in one of the two peaks.

4.3.3 Analysis

The formation of single adatoms with iron evaporation is a puzzling and unexpected result. Which element is forming the adatoms is not clear, as the iron-induced single adatoms are hardly distinguishable from indium adatoms in STM images. They have a similar height of around 100 pm and prefer the dark triangle sites. Even at a mixed coverages and under varying voltages, see figure 4.22, no differences are visible. The Fe atoms either form adatoms or switch places with In atoms of the surface layer, which then form adatoms.

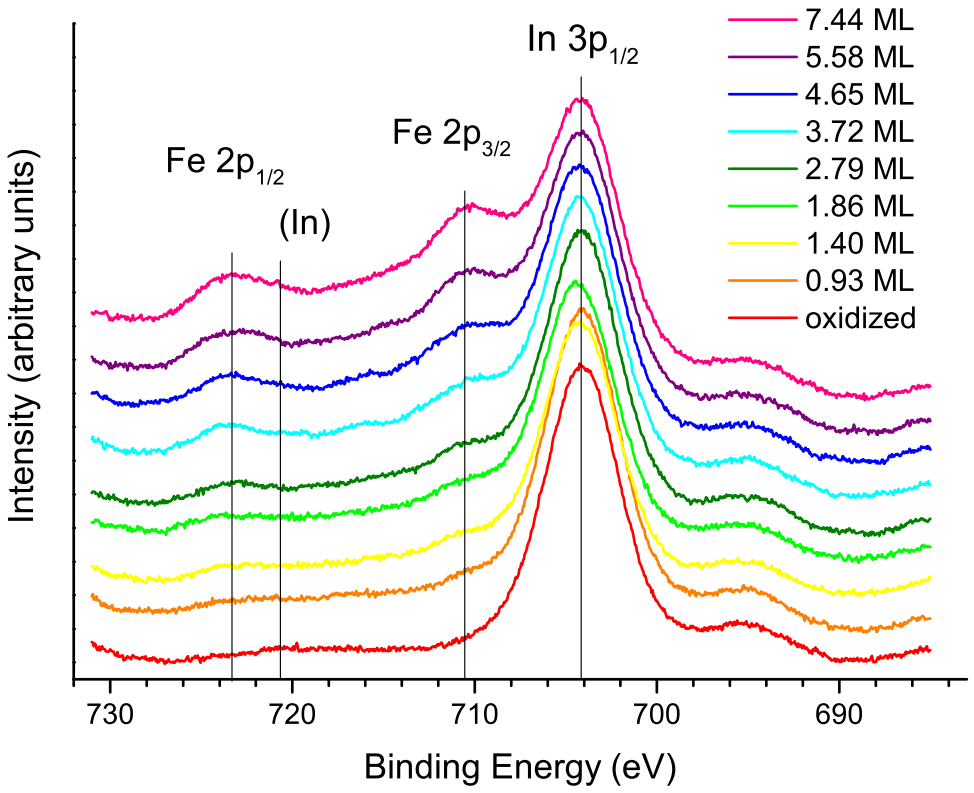

Figure 4.23: X-ray Photoelectron Spectroscopy measurement of the oxidized In_2O_3 (111) surface with rising coverages of iron, starting with the clean surface at the bottom and going up to 7.44 ML at the top. The iron peaks at 710.5 and 723.3 eV are visible above 1 ML of coverage. The indium peak at 704.2 eV is not visibly influenced by the evaporation. At 720.7 eV an In satellite peak is visible at lower coverages. The photon source used is a standard Mg Kα X-ray tube, emitting radiation at 1254 eV.

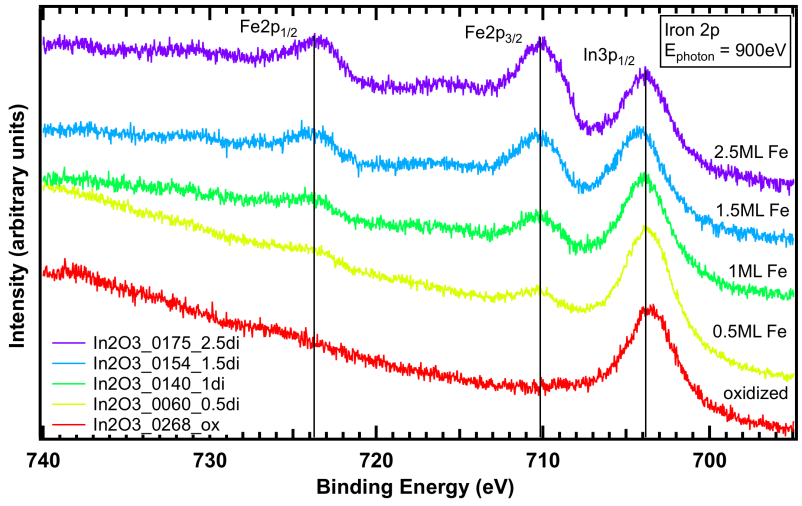

Figure 4.24: X-ray Photoelectron Spectroscopy measurement of the oxidized In_2O_3 (111) surface with increasing coverages of iron, starting with the clean surface at the bottom and going up to 2.5 ML at the top. The iron peaks are visible at all iron coverages. At 2.5 ML a metallic low-energy shoulder appears at approximately 709 eV which can be attributed to Fe^{2+}, see text. The $In3p_{1_2}$ peak at 704.7 eV shifts to 705.2 eV at the highest coverage. This shift could originate from band bending.

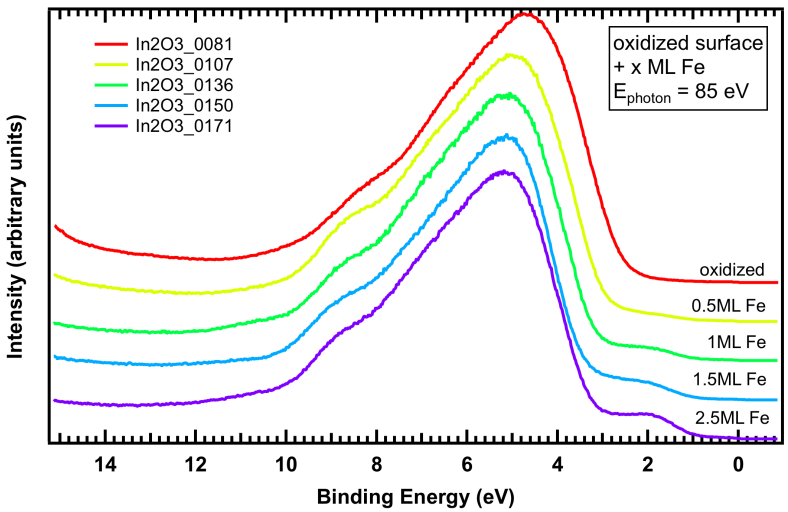

Figure 4.25: Valence band measurement of the oxidized In_2O_3 (111) surface with varying coverages of iron, using synchrotron radiation at 85 eV. The topmost spectrum was measured on the oxidized surface, the lowest with a coverage of 2.5 ML. At 2 eV a new peak appears in the band gap due to the iron coverage. The main peak at 4.7 eV shifts to 5.2 eV at the highest coverage. This could originate from band bending.

Although indium adatoms and adatoms formed after iron evaporation appear similar in STM images, differences can be found. The surface can not be filled with a full ordered (1x1) overlayer, as iron-induced adatoms become disordered above 0.6 ML. It is however possible to order coverages above 0.6 ML by heating the sample, see figure 4.19, where 0.7 ML were deposited. Annealing at 250 °C and above orders the adatoms perfectly. No additional adatoms appear at higher temperatures. Even at 425 °C, where a full monolayer of indium adatoms would be created on the oxidized surface, the coverage stays constant.

The disorder results from adatoms whose nearby dark triangle sites are blocked by other adatoms. After arriving on the surface, they cannot diffuse far enough to find an empty site. This can be seen in the disordered regime, where areas of disordered adatoms can be found near areas with few adatoms, see figure 4.17. In regions with high adatoms density, iron-induced adatoms have a tendency to form dimers such as in figure 4.20. Dimers are not commonly observed on reduced In_2O_3 surfaces.

Spectroscopic measurements can help to show whether iron is even present at the surface. The XPS measurements done with a standard Mg Kα X-ray source, see figure 4.23, show an iron peak, but only above one monolayer, which is a coverage in the disordered regime. Coverages in the ordered regime can be resolved when using synchrotron radiation as a photon source, see figure 4.24. Both XPS measurements have the drawback that they cannot be focused completely on our sample. The tantalum clip holders are measured to some extent, so iron next to the sample would compromise the results.

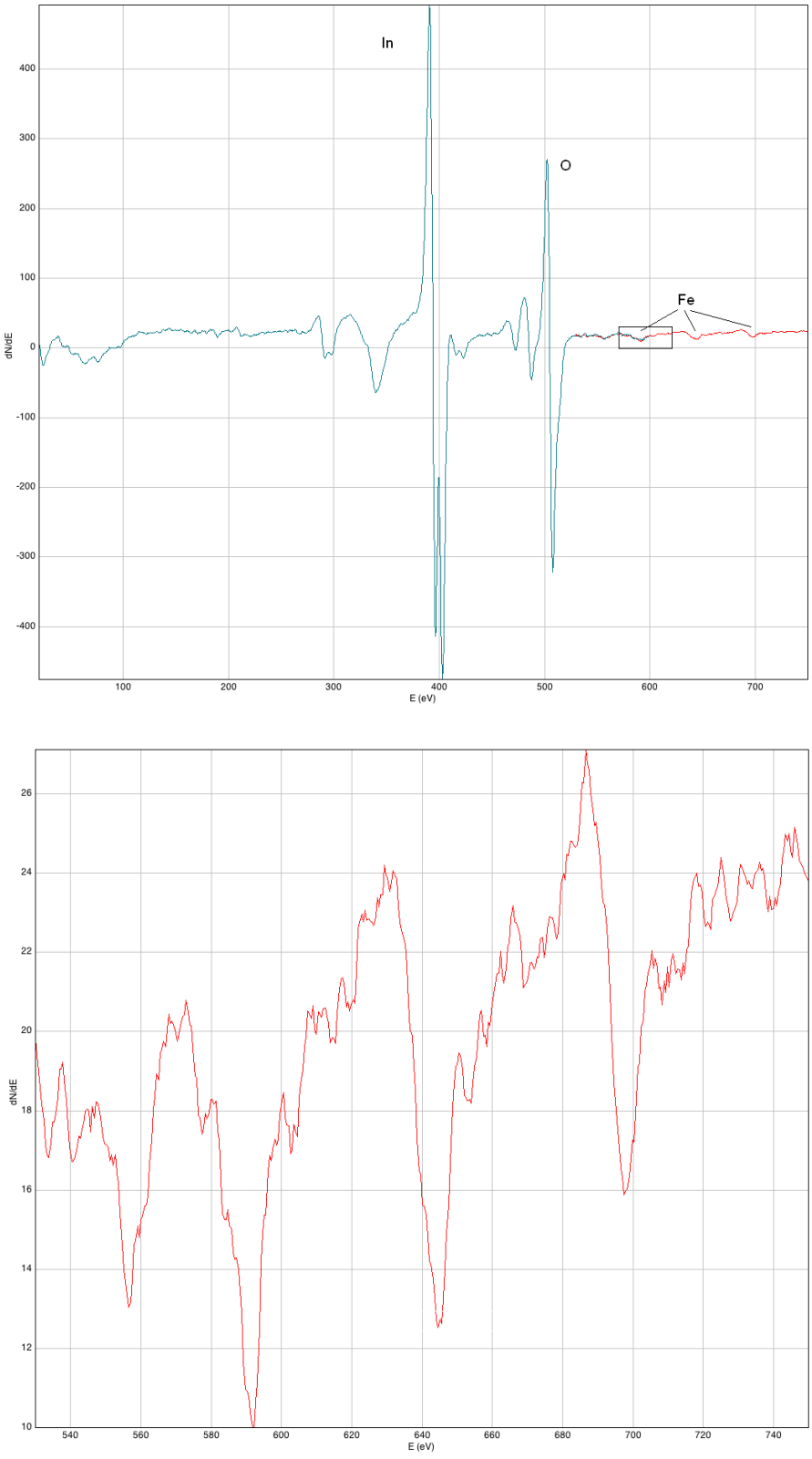

Figure 4.26: Auger Electron Spectroscopy measurement of the oxidized In_2O_3 (111) surface covered with 2.4 ML of iron. The upper figure shows the full differentiated spectrum in blue including the main peaks of oxygen (508 eV) and indium (at 396 and 403.5 eV) and a more detailed measurement of iron (592, 645 and 698 eV) in red. The lower figure shows the detailed iron measurement.

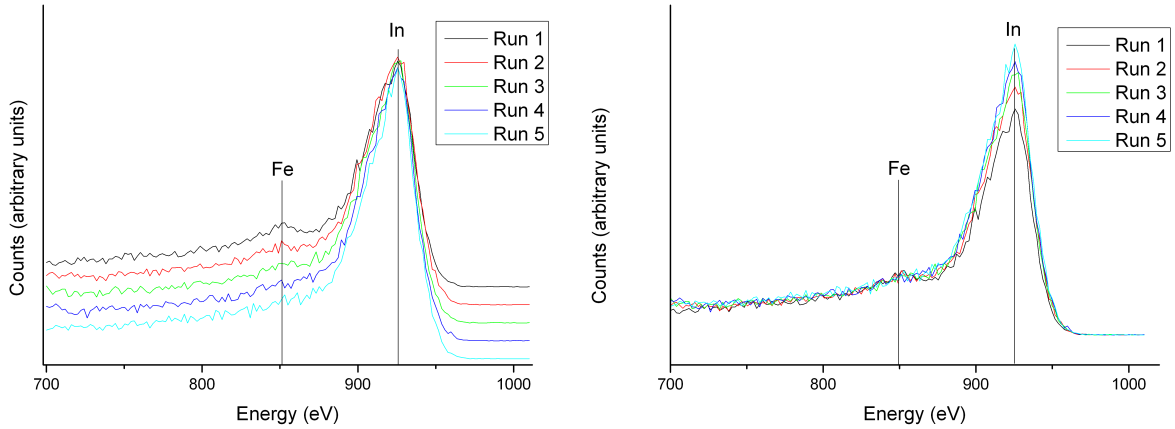

Figure 4.27: Low Energy Ion Spectroscopy measurement of the oxidized In_2O_3 (111) surface covered with 1 ML of iron. Both images show the same five runs of the measurement. On the left hand side, the spectra are shifted so that the decrease of the iron peak height becomes visible. On the right hand side the increase of the indium peak height is emphasized.

AES does not have this limitation, no tantalum signal is measured. In the AES measurement the coverage is high (2.31 ML), see figure 4.26, but it shows that iron can truly be found in the first layers of our sample. In the LEIS measurement at a coverage of 1 ML, see figure 4.27, the vanishing iron signal shows that iron atoms are present in the topmost surface layer. The spectroscopic measurements do however not show if iron forms the adatoms.

Further research is needed to show which option is correct: Iron forming adatoms or iron switching places with indium atoms, which then form adatoms. Possibilities for further investigations include DFT calculations and a challenging LEIS measurement with grazing angles to measure just the adatoms. In further STM measurements the tip could be used to remove adatoms and the surface below could be imaged to find Fe atoms in the first surface layer.

4.4 Nickel Deposition

After the outcome of the iron evaporation measurements, which lead to ordered adatoms, the question arose if other metals would yield the same result. The evaporation of nickel showed that nickel formed adatoms, but not in an ordered array.

Evaporating 0.35 monolayers nickel at room temperature on the oxidized In_2O_3 (111) surface resulted in disordered single adatoms. As shown in figure 4.28, two sites were preferred: Black triangle sites (similar to Fe adatoms) and sites between white triangles. In addition to agglomerations of adatoms at step edges were found, see figure 4.29. The adatoms were surrounded by dark rings. They appeared only 35 pm high, the trenches were 110 pm deep, see line profile in figure 4.29. These

dark rings are described by Sterrer *et al.* in [37] and by Repp *et al.* [38] as the results of negatively charged adatoms.

Note that these are preliminary results, further measurements have to be taken.

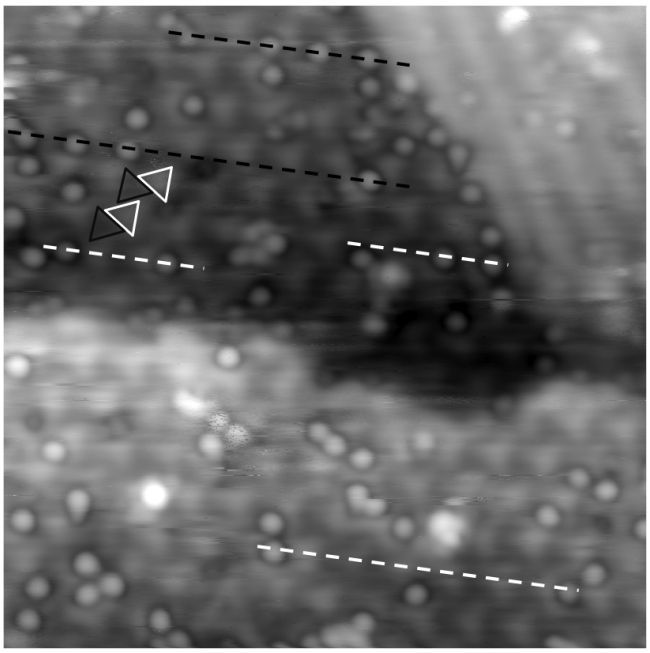

Figure 4.28: 20 x 20 nm^2, +2.1 V, 0.26 nA; data10078
The oxidized In_2O_3 (111) surface after evaporation of 0.35 ML of nickel at room temperature. The adatoms sit in dark triangle sites (examples indicated by black lines) or between bright triangle sites (white lines). In the top left corner the dark and bright triangles are indicated. The upper right terrace is created by a double tip.

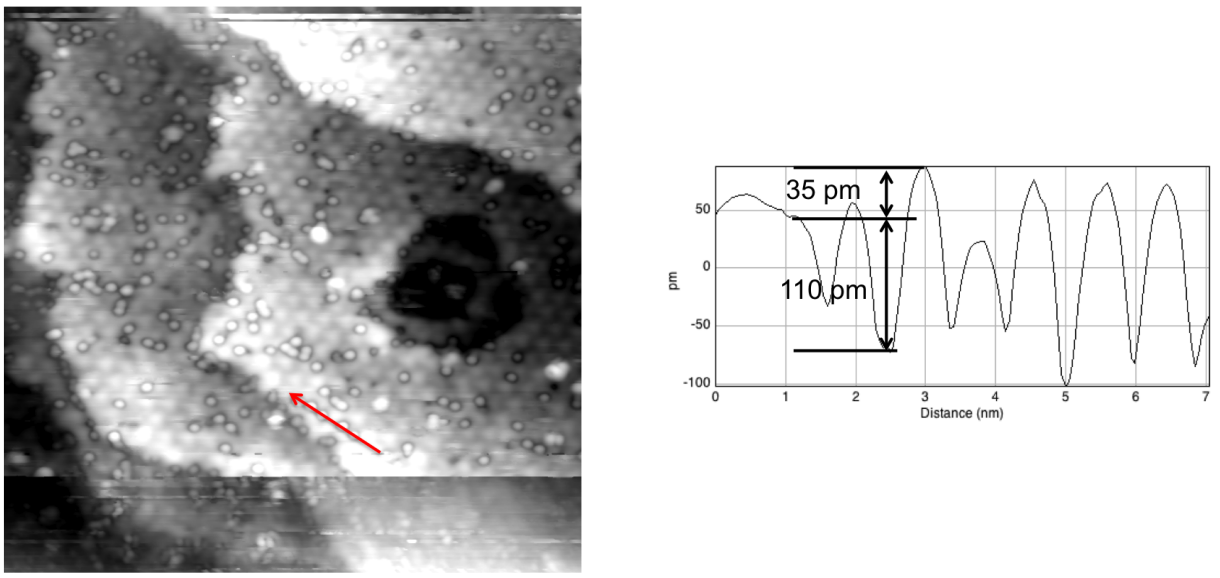

Figure 4.29: 40 x 40 nm^2, +1.2 V, 0.30 nA; data10066
The oxidized In_2O_3 (111) surface after evaporation of 0.35 ML of nickel. Some adatoms are agglomerated near the step edges. All adatoms are surrounded by a dark ring. The line profile shows an apparent adatom height of approximately 35 pm. The rings are 110 pm deep.

4.5 Deposition of Organic Molecules

Indium oxide is often used as an electrode material in organic semiconductor devices. The interaction between the In_2O_3 surface and organic molecules is important since it governs many properties of these devices. Two organic molecules, para-hexaphenyl (6P) and PTCDA were evaporated on the In_2O_3 (111) surface at room temperature. Models of the molecules can be found in chapter 2.4.5. At low coverages 6P formed lines of two molecules. At high coverages regions with ordered arrays were found. PTCDA formed single molecules at low coverages.

4.5.1 Para-Hexaphenyl (6P)

At low coverages 6P formed zig-zag lines of molecules, see figure 4.30. The molecules bonded strongly with the surface. They neither showed spontaneous mobility nor did they move during scanning.

The apparent length of one feature was between 3.8 and 4.3 nm, which was more than the length of one 6P-molecule (2.75 nm, van der Waals size, [20]). A feature therefore likely consisted of two folded molecules. Shorter features were found rarely.

The apparent height of the molecules was 80 pm, as is shown on the right side of figure 4.30, which is lower than a typical indium or iron adatom. The measured FWHM was 0.5 nm, in comparison with the literature value of 0.62 nm [20].

The two preferred directions of the molecules are shown in the small images of figure 4.30. The molecules were aligned along the diagonal of the surface unit cell and rotated by 120° to each other.

At coverages above one monolayer of 6P (uncalibrated QCM reading 2 Å), it was very difficult to image the surface using STM. No molecular features could be recognized (no image shown here). When heating this surface preparation to 190 °C however, some ordered regions appeared, see figure 4.31. In the ordered regions the 6P molecules aligned next to each other along the molecule's long axis. An ordered region typically consists of not more than ten molecules.

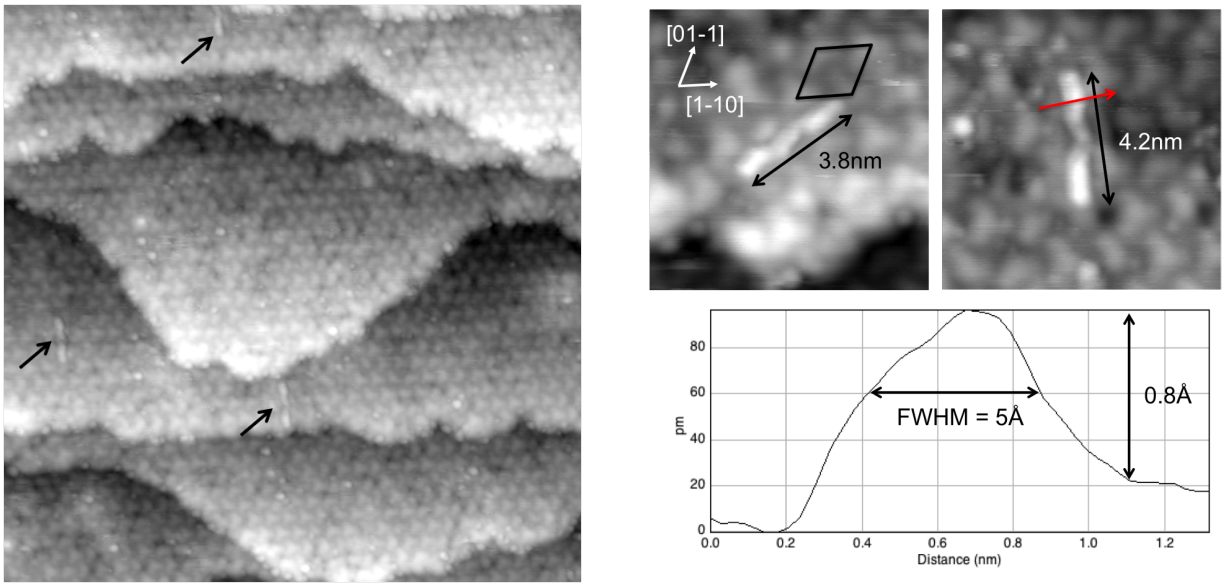

Figure 4.30: 50 x 50 nm^2, +1.2 V, 0.10 nA; data2424 8.5 x 8.5 nm^2, +1.2 V, 0.10 nA; data2422, 2421
The oxidized In_2O_3 (111) surface after evaporation of small amounts of 6P molecules. The surface is covered with several 6P molecules and a full layer of white triangle features originating from OH-groups. (left) 6P molecules are marked by arrows. (right) Two examples of 6P molecules. The unit cell and the surface directions are shown. Molecules are aligned along the diagonal of the unit cell. The line profile shows the apparent dimensions of the 6P molecule features: length 3.8 - 4.3 nm, height 0.8 Å, FWHM 5 Å.

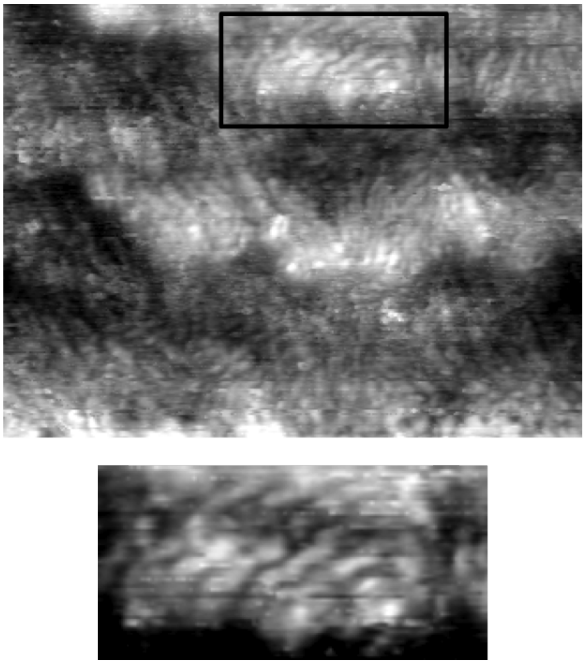

Figure 4.31: 48 x 64 nm^2 and zoomed, +1.5 V, 0.06 nA; data2404
The oxidized In_2O_3 (111) surface after evaporation of more than one monolayer of 6P molecules (2 Å, uncalibrated). Ordered and chaotic regions can be seen. The zoomed image shows an ordered region where molecules are aligned along their long axes.

4.5.2 PTCDA

Low amounts of perylene-3,4,9,10-tetracarboxylic-dianhydride (PTCDA) (uncalibrated QCM reading 0.2 Å) evaporated on the surface at room temperature resulted in singles molecules, see figure 4.32. On the right side the four most frequent directions of the molecules' long axes are drawn in yellow. Other orientations occurred rarely. The axes were determined using the work of Temirov *et al.* [39]. Four main alignments were found. No molecules aligned along the surface directions, marked with white arrows.

The molecules appeared about 2 Å high and measured 11 Å along the long axis and 13 Å along the short axis. Compared to the van der Waals size of 14.2 Å times 9.2 Å the ratio seems wrong. This however corresponds to the behavior described in [39], where the real long axis appears shorter than the short axis. The STM images in [39] show PTCDA that forms features similar to figure 4.32. After dosing hydrogen the contrast changes and the five rings of carbon atoms of PTCDA can be imaged and the long axis can be determined.

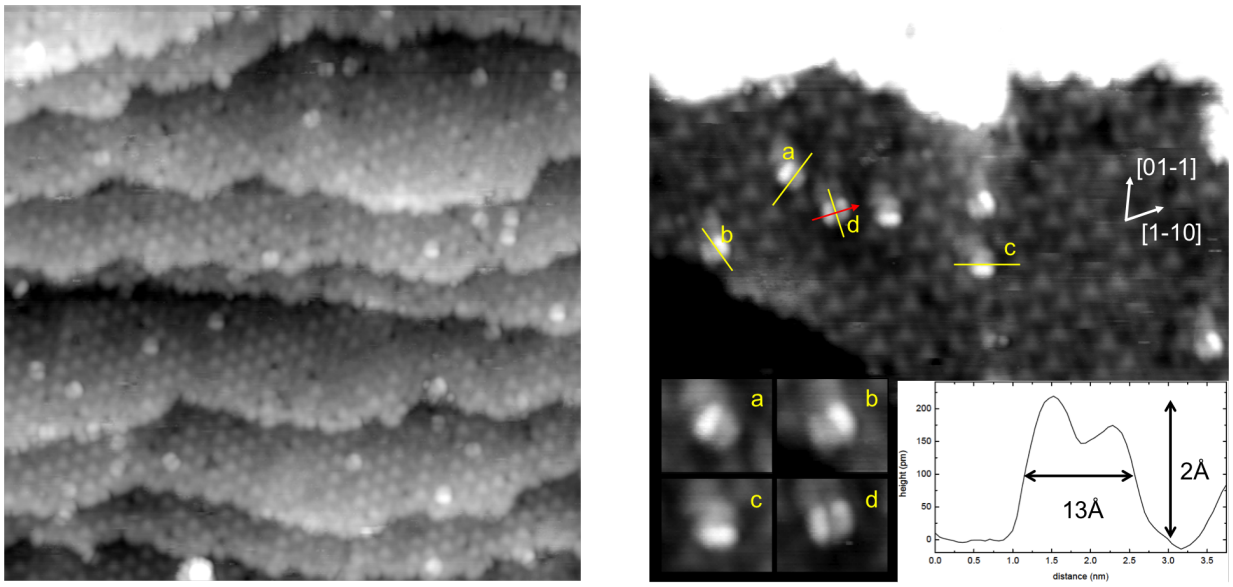

Figure 4.32: 50 x 50 nm^2, +2.4 V, 0.13 nA; data0012 30 x 30 nm^2, +1.7 V, 0.10 nA; data0022
The oxidized In_2O_3 (111) surface with single PTCDA molecules. On the left side PTCDA and water related white triangles can be seen. On the right side the four most frequent alignments of the molecules are marked in yellow. The base vectors of the surface unit cell are marked in white. In the bottom left corner the marked molecules are shown on a bigger scale. In the bottom right a line scan is shown, the position of the line scan is marked with a red arrow.

Chapter 5

Summary and Outlook

In this work, the adsorption of water, iron, nickel and organic molecules on In_2O_3 (111) was investigated with STM, XPS/UPS, AES and LEIS.

Dosing small amounts of water resulted in bright triangle-shaped features in STM measurements, which could be identified as OH-groups with XPS/UPS. In STM, the water related features have a specific adsorption site and appeared with the same shape and apparent height. They were able to hop to an equal neighboring site and left the normal, oxidized surface behind. At high coverages they formed a (1x1) overlayer. Spectroscopic measurements showed that a full monolayer consisted of two OH-groups per unit cell. Furthermore higher coverages of up to six OH-groups per unit cell were measured, but could not be observed with STM.

The discrepancies between STM and XPS measurements at high dosages of water should be investigated further using STM. There might be higher layers visible at coverages above several monolayers. DFT calculations could show if the OH adsorption site is energetically preferable as well as if one or more OH-groups form the observed white triangle features.

Using the reduction of one of the used single crystals, a theory on oxygen vacancies was tested. The predicted additional peak could not be confirmed. However, the In3d and O1s peaks were broader on the reduced crystal. The reason were final state effects due to a higher number of oxygen vacancies.

Iron evaporation up to coverages of 0.6 monolayers resulted in ordered arrays of adatoms. The adatoms were located in the same black triangle sites as indium adatoms of the reduced In_2O_3 (111) surface. Above 0.6 ML disordered regions appeared, which could be ordered by annealing at 250 °C. Bias dependent STM measurements did not show differences between In and Fe-induced adatoms when present simultaneously. The question arose whether the adatoms after Fe deposition were indeed Fe,

or rather In atoms which switched places with Fe. Spectroscopic measurements showed that iron was indeed on the surface or in the first surface layer.

The identity of the adatoms could not be solved so far, but ongoing DFT calculations are expected to shine more light on the interactions between Fe atoms and the In_2O_3 (111) surface. LEIS measurements under a grazing angle, to measure only the adatoms, would be a further possibility. AES and LEIS measurements could be done to show if iron remains in the topmost layer after annealing at 250 °C. In addition, In adatoms resulting from annealing in UHV could be compared with adatoms from Fe evaporation by investigating partial coverages with STM.

The evaporation of nickel also led to adatoms. The adatoms were not as ordered as after iron deposition and preferred two sites: The black triangles, like indium adatoms, and a site between white triangle features. In STM images the adatoms were surrounded by a dark ring that hints at negatively charged adatoms.

Two types of organic molecules were evaporated on the surface at room temperature: p-hexaphenyl (6P) and PTCDA. At low coverages 6P molecules in the STM images were aligned along the diagonal of the surface unit cell. The features were longer than the van der Waals length of one 6P molecule. A feature therefore likely consisted of two molecules. At high coverages the surface was difficult to image. After heating to 190 °C small ordered areas with up to 10 molecules appeared.

PTCDA formed single molecules at low coverages. The molecules showed preferred alignment axes differing from the surface unit cell axes.

The experiments on nickel, 6P and PTCDA presented in this thesis show first results, yet further STM as well as spectroscopic measurements have to be conducted to gain a better understanding of the ongoing processes.

Bibliography

[1] Kim H., Gilmore C., Pique A., Horwitz J., Mattoussi H., Murata H., Kafafi Z. and Chrisey D., *Electrical, optical, and structural properties of indium–tin–oxide thin films for organic light-emitting devices*: Journal of Applied Physics, 86(11):6451–6461 (1999)

[2] Patel N., Patel P. and Vaishnav V., *Indium tin oxide (ITO) thin film gas sensor for detection of methanol at room temperature*: Sensors and Actuators B: Chemical, 96(1):180–189 (2003)

[3] Forrest S.R., *"The path to ubiquitous and low-cost organic electronic appliances on plastic"*: Nature, 428:911–918 (April 2004)

[4] Ginley D., Hosono H. and Paine D.C., *Handbook of transparent conductors*: Springer Science & Business Media (2010)

[5] Granqvist C. and Hultåker A., *Transparent and conducting ITO films: new developments and applications*: Thin Solid Films, 411(1):1–5 (2002)

[6] Yang X.F., Wang A., Qiao B., Li J., Liu J. and Zhang T., *Single-Atom Catalysts: A new Frontier in heterogeneous catalysis*: Accounts of chemical research, 46(8):1740–1748 (2013)

[7] Parkinson G.S., Novotny Z., Argentero G., Schmid M., Pavelec J., Kosak R., Blaha P. and Diebold U., *Carbon monoxide-induced adatom sintering in a Pd–Fe3O4 model catalyst*: Nature materials, 12(8):724–728 (2013)

[8] Van de Leemput L. and Van Kempen H., *Scanning tunnelling microscopy*: Reports on Progress in Physics, 55(8):1165 (1992)

[9] Güntherodt H.-J. W.R., *Scanning tunneling microscopy I: general principles and applications to clean and adsorbate-covered surfaces*: Springer Verlag (1994)

[10] Moulder J.F., Stickle W.F., Sobol P.E. and Bomben K.D., *Handbook of X-ray photoelectron spectroscopy: a reference book of standard spectra for identification and interpretation of XPS data; Physical Electronics: Eden Prairie, MN, 1995*: Perkin-Elmer Corporation Physical Electronics Division (1992), ISBN 0-9627026-2-5

[11] Schmid M., *Experimentelle Methoden der Oberflächenphysik*: Vienna University of Technology (2015), summer term, (German)

[12] RHK Technology, *XPMPro 2.0 User's Guide*:

[13] Nyholm R., Andersen J., Johansson U., Jensen B. and Lindau I., *Beamline I311 at MAX-LAB: a VUV/soft X-ray undulator beamline for high resolution electron spectroscopy*: Nuclear Instruments and Methods in Physics Research Section A: Accelerators, Spectrometers, Detectors and Associated Equipment, 467:520–524 (2001)

[14] Als-Nielsen J. and McMorrow D., *Elements of Modern X-ray Physics*: Wiley (2011), ISBN 9781119970156

[15] Czanderna A., Joshi A., Davis L. and Palmberg P., *Methods of Surface Analysis. Chapter 5 - Auger electron spectroscopy*: Elsevier Science Publishing Co., New York (1989), ISBN 9780444596451

[16] Niehus H., Heiland W. and Taglauer E., *Low-energy ion scattering at surfaces*: Surface Science Reports, 17(4):213–303 (1993)

[17] Omicron Nanotechnology / Focus GmbH, *Omicron Instruction Manual, UHV Evaporator EFM 2/3/3s/4*: (August 2006), version 3.7

[18] OmniVac, *Users Manual 4-Pocket-Evaporator EV300*: 1st edition

[19] Wagner M., Seiler S., Meyer B., Boatner L.A., Schmid M. and Diebold U., *Reducing the In_2O_3 (111) Surface Results in Ordered Indium Adatoms*: Advanced Material Interfaces, 1 (November 2014), doi:10.1002/admi.201400289

[20] Resel R., Salzmann I., Hlawacek G., Teichert C., Koppelhuber B., Winter B., Krenn J., Ivanco J. and Ramsey M., *Structure and morphology of sexiphenyl thin films grown on aluminium (111)*: Organic electronics, 5(1):45–51 (2004)

[21] Glöckler K., Seidel C., Soukopp A., Sokolowski M., Umbach E., Böhringer M., Berndt R. and Schneider W.D., *Highly ordered structures and submolecular scanning tunnelling microscopy contrast of PTCDA and DM-PBDCI monolayers on Ag (111) and Ag (110)*: Surface science, 405(1):1–20 (1998)

[22] Marezio M., *Refinement of the crystal structure of In_2O_3 at two wavelengths*: Acta Crystallographica, 20(6):723–728 (1966)

[23] Hagleitner D.R., Menhart M., Jacobson P., Blomberg S., Schulte K., Lundgren E., Kubicek M., Fleig J., Kubel F., Puls C. *et al.*, *Bulk and surface characterization of In_2O_3 (001) single crystals*: Physical Review B, 85(11):115441 (2012)

[24] King P., Veal T.D., Fuchs F., Wang C.Y., Payne D., Bourlange A., Zhang H., Bell G.R., Cimalla V., Ambacher O. *et al.*, *Band gap, electronic structure, and surface electron accumulation of cubic and rhombohedral In_2O_3*: Physical Review B, 79(20):205211 (2009)

[25] Ágoston P., Erhart P., Klein A. and Albe K., *Geometry, electronic structure and thermodynamic stability of intrinsic point defects in indium oxide*: Journal of Physics: Condensed Matter, 21(45):455801 (2009)

[26] Morales E.H., He Y., Vinnichenko M., Delley B. and Diebold U., *Surface structure of Sn-doped In_2O_3 (111) thin films by STM*: New Journal of Physics, 10(12):125030 (2008)

[27] Zhang K., Payne D., Palgrave R., Lazarov V., Chen W., Wee A., McConville C.F., King P., Veal T.D., Panaccione G. *et al.*, *Surface structure and electronic properties of In_2O_3 (111) single-crystal thin films grown on Y-stabilized ZrO_2 (111)*: Chemistry of Materials, 21(19):4353–4355 (2009)

[28] Fan J.C. and Goodenough J.B., *X-ray photoemission spectroscopy studies of Sn-doped indium-oxide films*: Journal of Applied Physics, 48(8):3524–3531 (1977)

[29] Donley C., Dunphy D., Paine D., Carter C., Nebesny K., Lee P., Alloway D. and Armstrong N.R., *Characterization of indium-tin oxide interfaces using X-ray photoelectron spectroscopy and redox processes of a chemisorbed probe molecule: effect of surface pretreatment conditions*: Langmuir, 18(2):450–457 (2002)

[30] Kim J., Ho P., Thomas D., Friend R., Cacialli F., Bao G.W. and Li S., *X-ray photoelectron spectroscopy of surface-treated indium-tin oxide thin films*: Chemical Physics Letters, 315(5):307–312 (1999)

[31] Janowitz C., Scherer V., Mohamed M., Krapf A., Dwelk H., Manzke R., Galazka Z., Uecker R., Irmscher K., Fornari R. *et al.*, *Experimental electronic structure of In_2O_3 and Ga_2O_3*: New Journal of Physics, 13(8):085014 (2011)

[32] Morales E., *Growth and surface characterization of tin-doped indium oxide thin films*: (2010)

[33] Zhang H., *Structural and electronic investigations of In_2O_3 nanostructures and thin films grown by molecular beam epitaxy*: Oxford University (2012)

[34] Thiel P.A. and Madey T.E., *The interaction of water with solid surfaces: Fundamental aspects*: Surface Science Reports, 7(6):247–249 (1987)

[35] Henderson M.A., *The interaction of water with solid surfaces: fundamental aspects revisited*: Surface Science Reports, 46(1):10–15 (2002)

[36] Weiss W. and Ranke W., *Surface chemistry and catalysis on well-defined epitaxial iron-oxide layers*: Progress in Surface Science, 70(1):1–151 (2002)

[37] Sterrer M., Risse T., Pozzoni U.M., Giordano L., Heyde M., Rust H.P., Pacchioni G. and Freund H.J., *Control of the charge state of metal atoms on thin MgO films*: Physical review letters, 98(9):096107 (2007)

[38] Repp J., Meyer G., Olsson F.E. and Persson M., *Controlling the charge state of individual gold adatoms*: Science, 305(5683):493–495 (2004)

[39] Temirov R., Soubatch S., Neucheva O., Lassise A. and Tautz F., *A novel method achieving ultra-high geometrical resolution in scanning tunnelling microscopy*: New journal of physics, 10(5):053012 (2008)

Acknowledgment

I would like to express my gratitude to my supervisors, Margareta Wagner and Ulrike Diebold, for the useful comments and engagement through the learning process of this master thesis. I would like to thank Margareta for the good teamwork as well as the nonsense in between.

I would also like to thank Gareth Parkinson, who introduced me to the world of surface science. I am sorry that I could not enthuse you with skiing in return.

Special thanks go to Dr. Lynn A. Boatner, who provided the In_2O_3 crystals, and to the FWF (Project F45) and the ERC Grant "Oxide Surfaces" for the financial support.

Furthermore I would like to express my gratitude to everyone in the group for the nice hours and the support, especially while learning how to operate the vacuum chambers.

Many thanks to my family, especially my parents, for supporting me during the hard times and for showing me different perspectives.

Last but definitely not least I would like to thank Birgit Hasenberger for everything. For keeping me motivated, healthy, sane and most of all happy.